AMERICAN SOCIETY FOR MICROBIOLOGY | Microbiology Spectrum

RESEARCH ARTICLE

Genomic and Phenotypic Trait Variation of the Opportunistic Human Pathogen *Aspergillus flavus* and Its Close Relatives

E. Anne Hatmaker,[a,b] Manuel Rangel-Grimaldo,[c] Huzefa A. Raja,[c] Hadi Pourhadi,[c] Sonja L. Knowles,[c] Kevin Fuller,[d] Emily M. Adams,[d] Jorge D. Lightfoot,[d] Rafael W. Bastos,[e] Gustavo H. Goldman,[f] Nicholas H. Oberlies,[c] Antonis Rokas[a,b]

[a]Department of Biological Sciences, Vanderbilt University, Nashville, Tennessee, USA
[b]Evolutionary Studies Initiative, Vanderbilt University, Nashville, Tennessee, USA
[c]Department of Chemistry & Biochemistry, University of North Carolina at Greensboro, Greensboro, North Carolina, USA
[d]Department of Microbiology and Immunology, University of Oklahoma Health Science Center, Oklahoma City, Oklahoma, USA
[e]Biosciences Center, Federal University of Rio Grande do Norte, Natal, Brazil
[f]Faculdade de Ciências Farmacêuticas de Ribeirão Preto, Universidade de São Paulo, Ribeirão Preto, Brazil

ABSTRACT Fungal diseases affect millions of humans annually, yet fungal pathogens remain understudied. The mold *Aspergillus flavus* can cause both aspergillosis and fungal keratitis infections, but closely related species are not considered clinically relevant. To study the evolution of *A. flavus* pathogenicity, we examined genomic and phenotypic traits of two strains of *A. flavus* and three closely related species, *Aspergillus arachidicola* (two strains), *Aspergillus parasiticus* (two strains), and *Aspergillus nomiae* (one strain). We identified >3,000 orthologous proteins unique to *A. flavus*, including seven biosynthetic gene clusters present in *A. flavus* strains and absent in the three nonpathogens. We characterized secondary metabolite production for all seven strains under two clinically relevant conditions, temperature and salt concentration. Temperature impacted metabolite production in all species, whereas salinity did not affect production of any species. Strains of the same species produced different metabolites. Growth under stress conditions revealed additional heterogeneity within species. Using the invertebrate fungal disease model *Galleria mellonella*, we found virulence of strains of the same species varied widely; *A. flavus* strains were not more virulent than strains of the nonpathogens. In a murine model of fungal keratitis, we observed significantly lower disease severity and corneal thickness for *A. arachidicola* compared to other species at 48 h postinfection, but not at 72 h. Our work identifies variations in key phenotypic, chemical, and genomic attributes between *A. flavus* and its nonpathogenic relatives and reveals extensive strain heterogeneity in virulence that does not correspond to the currently established clinical relevance of these species.

IMPORTANCE *Aspergillus flavus* is a filamentous fungus that causes opportunistic human infections, such as aspergillosis and fungal keratitis, but its close relatives are considered nonpathogenic. To begin understanding how this difference in pathogenicity evolved, we characterized variation in infection-relevant genomic, chemical, and phenotypic traits between strains of *A. flavus* and its relatives. We found extensive variation (or strain heterogeneity) within the pathogenic *A. flavus* as well as within its close relatives, suggesting that strain-level differences may play a major role in the ability of these fungi to cause disease. Surprisingly, we also found that the virulence of strains from species not considered to be pathogens was similar to that of *A. flavus* in both invertebrate and murine models of disease. These results contrast with previous studies on *Aspergillus fumigatus*, another major pathogen in the genus, for which significant differences in infection-relevant chemical and phenotypic traits are observed between closely related pathogenic and nonpathogenic species.

KEYWORDS *Aspergillus flavus*, genomes, phenotypic variation, secondary metabolites, fungal keratitis, aspergillosis, biosynthetic gene cluster, comparative genomics, evolution, genomics, pathogenicity, secondary metabolism

Editor Alexandre Alanio, Institut Pasteur

Address correspondence to Antonis Rokas, antonis.rokas@vanderbilt.edu.

The authors declare a conflict of interest. A.R. is a scientific consultant for LifeMine Therapeutics, Inc., and N.H.O. is a member of the Scientific Advisory Board of Mycosynthetix, Inc.

Received 31 August 2022
Accepted 10 October 2022
Published 1 November 2022

Fungal infections affect millions of people worldwide annually but remain understudied and poorly understood (1). Severe fungal infections in humans, such as aspergillosis, commonly affect immunocompromised individuals (2). Invasive aspergillosis is an umbrella term describing a range of respiratory infections caused by inhalation of asexual spores of several *Aspergillus* species that grow into human tissue (3). Around 300,000 cases of invasive aspergillosis are identified each year, with a high mortality rate (2). Another form of aspergillosis, chronic pulmonary aspergillosis, impacts ~3 million people annually (2). Invasive aspergillosis and chronic pulmonary aspergillosis can also co-occur in immunocompetent patients with severe viral infections, such as severe acute respiratory syndrome coronavirus 2 (4) and influenza virus (5).

Fungal keratitis, or inflammation of the cornea due to a fungal infection, affects otherwise-healthy individuals, although immunocompromised individuals have higher rates of infection than immunocompetent ones (2). Globally, at least 1,000,000 cases of fungal keratitis occur annually, including both yeast and filamentous fungal infections (2), over 15,000 of which are in the United States, and ~10% of cases result in eye removal due to late diagnosis or poor therapeutic outcomes (6). Fungal keratitis can lead to blindness, and affected individuals are typically infected through small wounds on the eye's surface (7). The disease primarily afflicts outdoor workers (e.g., farmers) and contact lens wearers (8, 9). Sand and vegetative material often cause the initial wounds through which the infection spreads (10). In western countries, including in the United States, contact lens use is the primary risk factor (11). The Global Action Fund for Fungal Infections has designated fungal keratitis a public health priority (12). Childhood fungal keratitis is the most frequent cause of corneal blindness worldwide (13), which occurs in 40% of severe fungal keratitis cases (12).

Aspergillus flavus, an opportunistic human pathogen, is estimated to cause 10% of invasive aspergillosis infections worldwide, second only to *Aspergillus fumigatus*, and up to 80% of keratitis infections from *Aspergillus* species (14). Retrospective studies from Cuba and Pakistan identified more cases of chronic pulmonary aspergillosis caused by *A. flavus* than other *Aspergillus* species (15, 16). *A. flavus* is widespread in the environment, particularly in tropical regions (17), but we do not currently know which *A. flavus* traits impact virulence in humans. The taxonomic section *Flavi* includes *A. flavus* and closely related species such as *Aspergillus parasiticus*, *Aspergillus arachidicola*, and *Aspergillus nomiae* (18). Species in section *Flavi* share several morphological characteristics (19), including production of the carcinogen aflatoxin (18), but do not cause human disease at similar rates (20). Throughout this report, we use "nonpathogenic" to refer to species rarely or never isolated from human or animal infections and which are not considered clinically relevant.

A. flavus is more commonly isolated in invasive aspergillosis and fungal keratitis cases than its close relative *A. parasiticus* (17). Okun et al. (21) observed similar geographic ranges for the two species in agricultural fields in Kenya, although *A. flavus* was isolated about twice as often (63% of all isolates were *A. flavus* versus 28% *A. parasiticus*). In the western United States, prevalence and occurrence density of the two species varied based on location, with 48% of *Aspergillus* isolates identified as *A. parasiticus* at some sampling locations (22). Despite the prevalence of *A. parasiticus* in the environment, the species is rarely isolated from patients, deviating from expectations based on species distribution and density data, indicating additional factors may be necessary for human pathogenicity. We note that *A. parasiticus* has been occasionally identified as a causal agent of human infections, but these infections occur at a much lower rate than those caused by *A. flavus*, and we were unable to identify published case studies.

A. flavus and *A. parasiticus* also both grow well at 37°C and 42°C (23); thermotolerance is considered key for *Aspergillus* pathogenicity in general (24, 25). Growth at 37°C has also been shown to change the metabolic profile of *Aspergillus* species (26). Secondary metabolites, which are small organic molecules with potent bioactivities, enable fungi to augment their environment with defensive compounds (27) and can impact virulence by modulating host biology (28, 29), as with gliotoxin in *A. fumigatus* (30). *A. flavus* and other section *Flavi* species have an even larger arsenal of secondary metabolites than *A. fumigatus* (31).

Temperature can also impact secondary metabolite production. At 37°C, *A. flavus* produces diverse secondary metabolites (32). At lower temperatures, the most notable *A. flavus* secondary metabolite is the mycotoxin aflatoxin, a carcinogen (32), which is also produced by several other section *Flavi* species, including *A. parasiticus* (18). *A. flavus* is also predicted to produce scores of other secondary metabolites (33) which may play a role in human infection.

Current knowledge of *A. flavus* molecular mechanisms involved in human virulence relies heavily on extrapolation from studies of an *A. fumigatus* mouse models of both fungal keratitis (34) and respiratory infections (35) rather than direct studies of *A. flavus*, despite extensive genomic and phenotypic differences between the two species. Although in the same genus, *A. flavus* and *A. fumigatus* are not close relatives and are in distinct taxonomic sections of *Aspergillus*, sections *Flavi* and *Fumigati*, respectively (18); at the level of genome sequence divergence, the two species are as similar to each other as humans are to fish (36). Compared to *A. fumigatus*, section *Flavi* species have, on average, larger genomes, encode more genes, and are predicted to contain more biosynthetic gene clusters (BGCs) involved in the biosynthesis of secondary metabolites (37). Differences between *A. flavus* and *A. fumigatus* include resistance to antifungal drugs, as azole resistance differs between the two species, with triazole resistance considered rare in *A. flavus* despite comparable exposure to environmental fungicides as *A. fumigatus* (38). Additional studies investigating genetic determinants of virulence specific to *A. flavus*, which enable the species to infect humans at a higher rate than closely related species, as well as the drug resistance profiles of diverse strains and species, are needed to better understand the pathogenicity of *A. flavus*.

To begin addressing the evolution of pathogenicity in section *Flavi*, we examined the genomes, secondary metabolite profiles, and other infection-relevant phenotypic traits (e.g., virulence) of two *A. flavus* strains and strains from three closely related species that rarely infect humans: *A. arachidicola* (two strains), *A. parasiticus* (two strains), and *A. nomiae* (one strain). The species were chosen based on their phylogenetic placement within the section and close evolutionary affinity, their difference in clinical relevance, and shared characteristics with *A. flavus*, such as aflatoxin production. We sequenced seven strains from the four species and identified proteins unique to *A. flavus* strains, including BGCs absent in the nonpathogenic species. Temperature impacted secondary metabolite production in all four species, but secondary metabolites unique to *A. flavus* were not identified under these conditions. Antifungal drug resistance did not differ appreciably between strains or species, but strains of the same species exhibited variation in growth under certain stress conditions. Evaluation of virulence using an invertebrate model of disease revealed additional variations between strains of the same species, and *A. flavus* strains were not the most virulent in this model. Virulence in a murine model of fungal keratitis was tested with one strain each from *A. flavus*, *A. parasiticus*, and *A. arachidicola*, along with a reference strain of *A. fumigatus*, revealing significantly lower disease severity and corneal thickness in mice infected with *A. arachidicola* compared to those infected with the other species. The combination of genomic and phenotypic comparisons revealed similarities and differences between *A. flavus* and three nonpathogenic close relatives within *Aspergillus* section *Flavi*. This study provides key data on the genomic, chemical, and phenotypic diversity of closely related pathogenic and nonpathogenic species in *Aspergillus* section *Flavi* that further our knowledge of how some of these fungi can opportunistically infect humans.

RESULTS

Draft genomes for seven strains of *A. flavus* and nonpathogenic close relatives. We sequenced and assembled seven genomes from four species with high coverage (81× to 230×). The *A. flavus* NRRL 1957 draft genome consisted of the fewest scaffolds (143), whereas the draft genome of *A. arachidicola* IC26646 had the most (1,440). *A. nomiae* NRRL 6108 had the smallest genome, at 36.8 Mbp, and *A. parasiticus* NRRL 502 had the largest, at 41.4 Mbp; *A. flavus* strains had smaller genomes than strains of *A.*

TABLE 1 Genome sequencing, assembly, and annotation for the seven strains of four *Aspergillus* species revealed expected genome size and good coverage depth

Species	Strain	Total paired reads	Trimmed paired reads	No. of scaffolds	N_{50}	Coverage	Size (Mbp)	No. of predicted proteins
Aspergillus arachidicola	IC26645	30,016,585	28,186,702	805	1,139,563	102×	41.2	13,710
Aspergillus arachidicola	IC26646	32,284,138	29,911,439	1,440	1,298,300	109×	40.9	13,731
Aspergillus flavus	NRRL 1957	44,750,116	40,985,045	143	1,892,429	163×	37.6	14,216
Aspergillus flavus	NRRL 501	30,987,721	28,845,216	563	1,420,800	111×	38.8	13,997
Aspergillus nomiae	NRRL 6108	25,466,314	23,606,091	252	1,660,546	96×	36.9	11,820
Aspergillus parasiticus	NRRL 502	24,439,029	22,469,327	702	95,7843	81×	41.5	13,470
Aspergillus parasiticus	NRRL 2999	63,194,489	62,404,154	516	1,838,014	230×	40.6	13,590

parasiticus or *A. arachidicola* (Table 1). All genomes had over 93% of the expected universal single-copy orthologs (Table 2).

Placement of newly sequenced genomes consistent with *Aspergillus* section *Flavi* phylogeny. Our maximum likelihood species tree was built from 2,422 orthologs shared among 20 *Aspergillus* species (Fig. 1). Species identification was confirmed for all the newly sequenced strains (NRRL 501, 502, 1957, 2999, and 6108 and IC26645 and IC26646) with high support (bootstrap replicates = 100), with each strain placed among the representative strains of the expected species (Table 1). We noted that previous whole-genome sequencing of a strain labeled NRRL 2999 (GCA_012897115.1) was recently determined to be *A. flavus* rather than *A. parasiticus* (39) and was acknowledged as a clonal derivative of *A. flavus* NRRL 3357 (40). Our NRRL 2999 strain and *A. parasiticus* SU-1 share 99.98% average nucleotide identity, confirming that our strain, obtained from the NRRL culture collection, is *A. parasiticus*.

More than 3,000 protein families are unique to the pathogen *A. flavus*. We identified 8,717 protein families shared by all seven newly sequenced strains (Fig. 2). A further 3,054 protein families were present in both *A. flavus* strains but absent from the other five strains. This group of protein families was enriched for the gene ontology (GO) terms GO:0016705 oxidoreductase activity (15 protein families; $P < 0.0001$, hypergeometric distribution) and GO:0055085 transmembrane transport (30 protein families; $P < 0.0001$). *A. arachidicola* strains shared 3,097 unique protein families enriched for GO term GO:0016114 terpenoid biosynthetic process (10 protein families; $P < 0.00001$), and *A. parasiticus* strains shared 1,230 unique protein families without any GO term enrichment. No GO terms were enriched within the 1,322 protein families unique to *A. nomiae*.

We also examined the number of orthogroups (predicted protein families) shared among and within species for all 20 species and 30 strains by using the OrthoFinder results. All 20 species, including the outgroup *Aspergillus niger*, shared 3,861 orthogroups, and 388 orthogroups were in all section *Flavi* species but absent in *A. niger* (see Fig. S1 in our supplementary information, available on the FigShare website [https://doi.org/10.6084/m9.figshare.20256336]). The number of orthogroups unique to any particular strain ranged from 229 to 281 (see Fig. S1), which was consistent with our analysis of the 7 strains phenotyped in this study. For example, 280 strain-specific orthogroups were identified for *A. parasiticus* NRRL 502 in the

TABLE 2 Genome completeness assessment of draft *Aspergillus* genomes sequenced for this study

Species	Strain	No. of BUSCOs[a]				
		Present (%)	Complete	Duplicated	Fragmented	Missing
Aspergillus arachidicola	IC26645	97.1	4,072	14	40	79
Aspergillus arachidicola	IC26646	97.0	4,065	14	41	85
Aspergillus flavus	NRRL 1957	95.9	4,023	48	53	115
Aspergillus flavus	NRRL 501	96.0	4,023	19	52	116
Aspergillus nomiae	NRRL 6108	93.1	3,607	16	158	410
Aspergillus parasiticus	NRRL 502	97.8	4,099	15	21	71
Aspergillus parasiticus	NRRL 2999	98.0	4,105	15	21	65

[a]BUSCO, benchmarking universal single-copy orthologs.

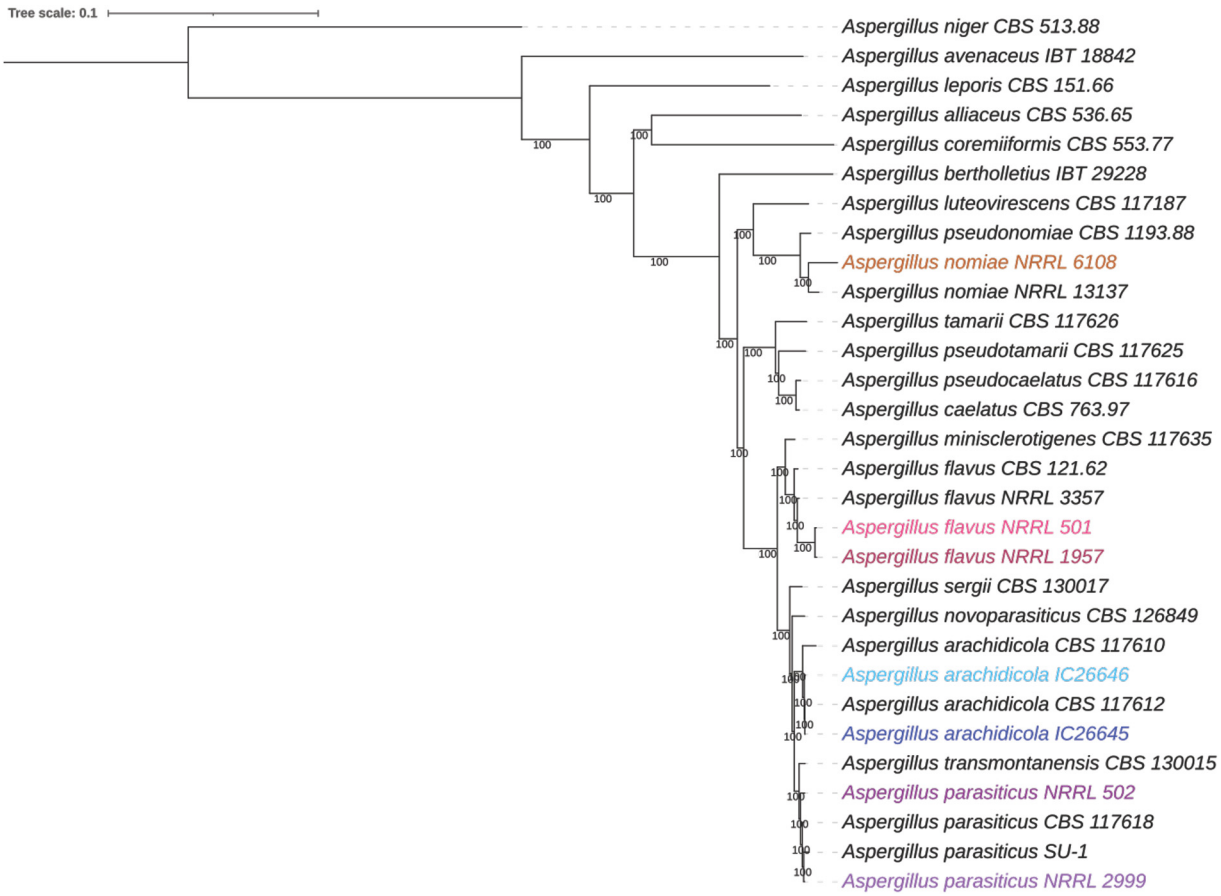

FIG 1 The taxonomic identity of newly sequenced strains was consistent with *Aspergillus* section *Flavi* phylogeny. A maximum likelihood phylogeny was constructed using 2,422 single-copy orthologs from 30 strains of 20 *Aspergillus* species, with *A. niger* as the outgroup. Additional information about strains used can be found in Table 5. Numbers near branches are bootstrap values calculated from 1,000 replicates. Strains sequenced as part of this study are highlighted, with *A. nomiae* NRRL 6108 in orange, *A. flavus* in pink (NRRL 501 in light pink, NRRL 1957 in dark pink), *A. arachidicola* in blue (IC26645 in dark blue, IC26646 in light blue), and *A. parasiticus* in purple (NRRL 502 in dark purple, NRRL 2999 in light purple).

larger analysis that included all 30 strains, whereas 283 were identified in the smaller analysis that included only 7 strains (Fig. 2). From our examination of all 30 strains, 1,991 orthogroups were unique to *A. flavus* strains, compared to over 3,000 orthogroups identified in the 7-strain analysis. No orthogroups were absent in *A. flavus* but present in all other species.

Many predicted biosynthetic gene clusters and secondary metabolites were shared between species. Using the fungal version of antiSMASH, we predicted biosynthetic gene clusters (BGCs) from the seven strains. *A. nomiae* NRRL 6108 had the fewest predicted BGCs at 49, whereas *A. parasiticus* strains had the most predicted BGCs, as NRRL 2999 and NRRL 502 were predicted to contain 80 and 81 BGCs, respectively. Both *A. arachidicola* strains encoded more predicted BGCs (76 for IC26645 and 73 for IC26646) than either *A. flavus* strain, but fewer than either *A. parasiticus* strain. Our two *A. flavus* strains, NRRL 1957 and NRRL 502, encoded 70 and 71 BGCs, respectively (Fig. 3A). Of these BGCs, 44 (NRRL 1957) and 45 (NRRL 502) were not linked to any known metabolites.

A total of 118 BGC families were present in the seven strains, with 24 families shared by all strains and 7 families unique to the *A. flavus* strains (Fig. 3C). Eight additional BGC families were identified in all strains but *A. nomiae* (see Table S1 in our supplementary information [https://doi.org/10.6084/m9.figshare.20256336]). Our *A. flavus* strains shared 58 BGC families (see Table S1).

Genetic determinants of virulence were present in all species. Through a review of the literature, we identified 50 genes related to virulence or sporulation in *A. flavus* (29, 31–72). The majority of the genetic determinants of virulence have been studied

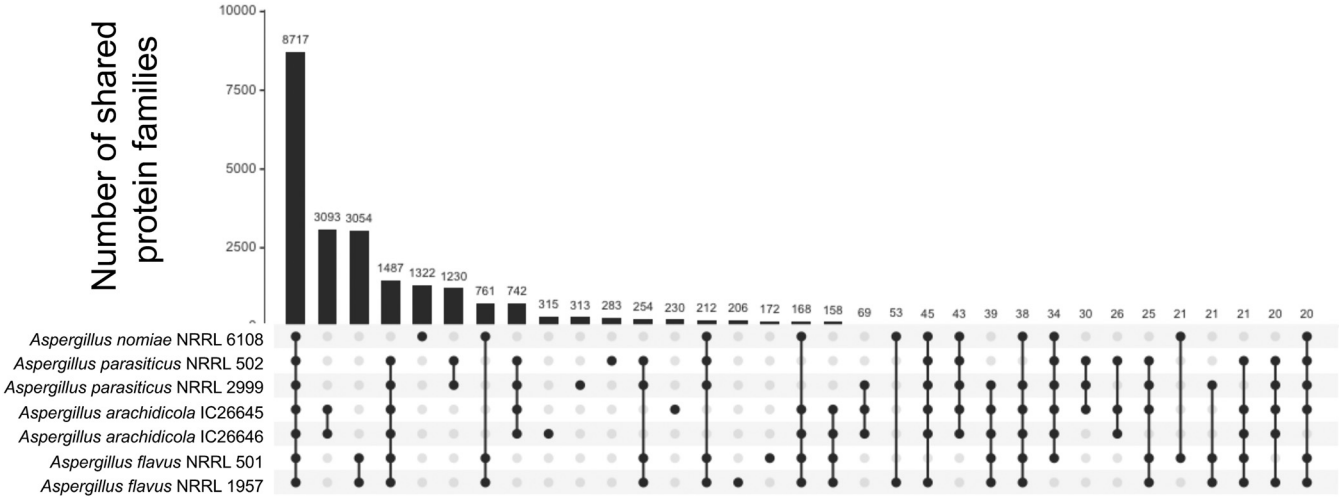

FIG 2 Strains of the same species did not differ substantially in number of predicted protein families present in their genomes. Upset plot shows the number of shared protein families for orthogroups with at least 20 proteins. Linked black circles under the bar plot indicate strains sharing orthologous protein families. Numbers above bars indicate exact numbers of shared families.

only in the context of plant pathology, with seed infection and asexual spore (conidia) count assays, although six genes have been tested in animal models of fungal disease (Fig. 4). Several studies implicated aflatoxin biosynthesis in *A. flavus* plant pathogenesis, linking virulence and aflatoxin production. With the exception of genes involved in the aflatoxin biosynthetic gene cluster, which are absent in *A. flavus* NRRL 501, all 50 genetic determinants of virulence were identified in all seven strains (Fig. 4). Of the genes identified, 12 were orthologous to genetic determinants of virulence for *A. fumigatus* (see Table S2). An additional stress response protein, *sfgA*, which plays an important role in rendering *A. flavus* more stable to the external environment (73), was also found in all seven strains.

Strains had heterogeneous secondary metabolite profiles. Evaluation of the secondary metabolite profiles of the seven fungi at both room temperature and 37°C, with or without the inclusion of saline, led to several key observations. First, the inclusion or absence of saline had little to no effect on the secondary metabolite profiles, as major differences were not observed between strains grown under the same conditions (i.e., room temperature or 37°C) both with and without physiologic saline (see Fig. S2 and S3 in our supplementary information [https://doi.org/10.6084/m9.figshare.20256336]). Therefore, our analysis of secondary metabolites focused on the impact of temperature. Each strain produced a unique set of metabolites, particularly at room temperature, and this held true even for strains of the same species (Table 3). A principal-component analysis (PCA) revealed that *A. parasiticus* strains NRRL 2999 and NRRL 502 were most differentiated along principal component two at 37°C, explaining ~24% of the variation (Fig. 5A). Conversely, strains of *A. arachidicola* were more similar to each other at 37°C than at room temperature, as were strains of *A. flavus* (Fig. 5).

In general, the cultures grown at room temperature contained a high proportion of mycotoxins (i.e., compounds **1** to **32**) or ergosterol derivatives (**33**), whereas the cultures grown at 37°C had a much higher concentration of metabolites derived from fatty acids (i.e., compounds **34** to **68**) (further details for compounds **1** to **68** have been submitted to the Natural Products Magnetic Resonance Database [https://np-mrd.org/]). Interestingly, the two strains of *A. flavus* (i.e., NRRL 501 and NRRL 1957) did not share any compounds in their secondary metabolite profiles when grown at room temperature. Moreover, other than leporin B and C (compounds **10** and **11**, respectively) and cyclopiazonic acid (**18**), the secondary metabolite profiles of the two strains of *A. flavus* did not overlap with the secondary metabolite profiles of any of the other section *Flavi* species when grown at room temperature. *A. flavus* NRRL 501 largely biosynthesized aspergillic acid (**29**) and a variety of related analogs, confirming previous

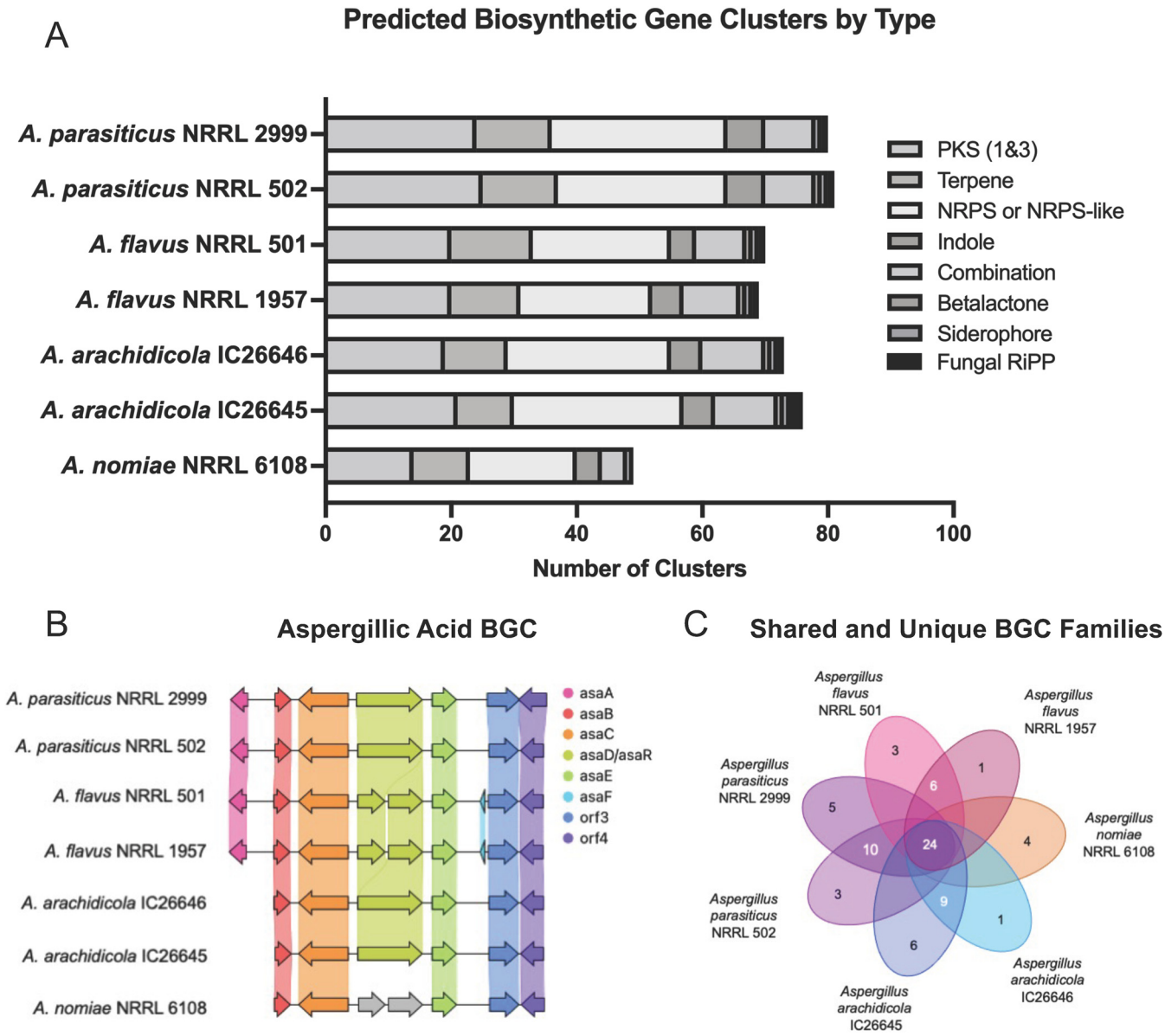

FIG 3 Strains of the same species did not differ substantially in their predicted biosynthetic gene clusters (BGCs). (A) Stacked bar plot of predicted BGCs. Each bar adds up to the total number of predicted BGCs, with the type of BGC indicated by color. (B) Synteny plot comparison of the aspergillic acid BGC from all seven strains. Arrows represent genes, and vertically shaded areas between arrows indicate sequence similarity. (C) Diagram of unique (singletons) and shared BGC families, calculated by BiGSCAPE.

reports (74), whereas *A. flavus* strain NRRL 1957 biosynthesized cyclopiazonic acid (**18**) and a range of analogs, such as speradines A (**19**), C (**21**), F (**22**), I (**23**), and H (**24**) and asperorydine H (**25**). Additionally, this strain biosynthesized indol-terpenoids, such as paspaline (**26**) and aflatrem (**27**).

A. parasiticus NRRL 2999 and *A. arachidicol*a IC26645 had very similar secondary metabolite profiles and were prolific producers of aflatoxins B1 (**1**), B2 (**2**), G1 (**3**), and G2 (**4**), astellolids A (**6**), B (**7**), and D (**8**), and leporins B (**10**) and C (**11**), along with some minor metabolites, such as aspergillicin A (**12**) and phomaligol A (**13**). In contrast, *A. parasiticus* NRRL 502 and *A. arachidicola* IC26646 did not biosynthesize aflatoxins or leporins. However, *A. parasiticus* NRRL 502 produced astellollids A (**6**) and B (**7**) and polyketides like phomaligol A (**13**), phomagilin A (**14**), and aspersitin (**15**), whereas the latter (i.e., *A. arachidicola* IC26646) only produced the 14-deacetyl derivative of astellolide A (**9**) and traces of aspergillicin A (**12**) and phomaligol A (**13**). Furthermore, we

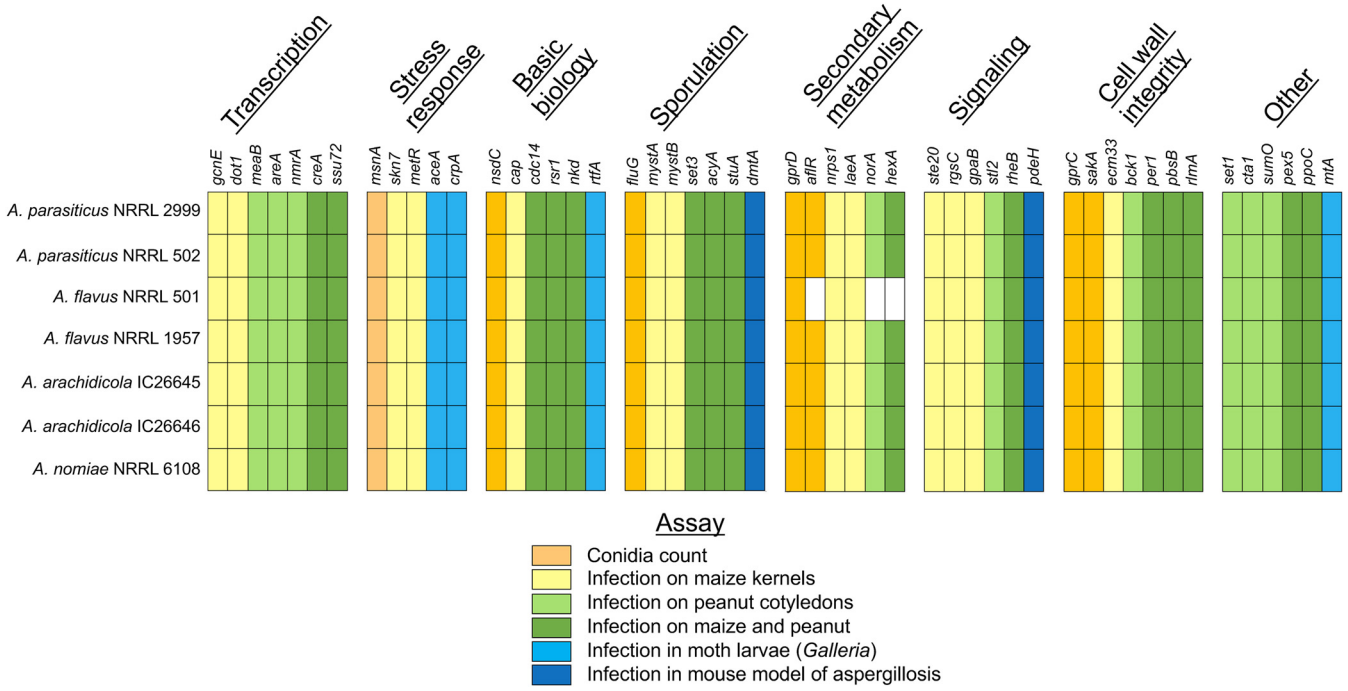

FIG 4 Genetic determinants of virulence were identified in all strains; data shown here summarize presence or absence of 50 *Aspergillus flavus* genetic determinants of virulence. All genes were identified in all strains except *aflR*, *norA*, and *hexA*, which were absent in *A. flavus* NRRL 501. Colors represent the *A. flavus* experimental virulence assay for each gene (from published literature). Genes which were studied using an animal model are in shown in light or dark blue. Additional information is provided in Table S2 of our supplementary information on the FigShare website.

observed that *A. nomiae* NRRL6108 biosynthesized a smaller suite of mycotoxins, which was consistent with the smaller number of predicted BGCs in its genome; however, it uniquely produced *O*-methylsterigmatocystin (**5**) and parasiticol (**16**), two metabolites closely related to aflatoxins and likely derived from similar BGCs.

The isolated metabolites at 37°C were largely composed of fatty acids (mostly C_{18} and C_{16} derivatives), particularly the sporogenic PSI (precocious sexual inducer) factors A, B and C (i.e., **41** to **45**). These compounds were found in all the strains grown at 37°C. A few of the mycotoxins were also observed at elevated temperatures, specifically astellolids A (**6**) and B (**7**) in *A. parasiticus* NRRL 2999 and *A. arachidicola* IC26645 and *O*-methylsterigmatocystin (**5**) in *A. nomiae* NRRL 6108. In total, the results showed a surprising amount of heterogeneity of the secondary metabolomic profiles both between species and even between strains of the same species. Structures for all identified metabolites are available in our supplementary information on FigShare (Table S3) and were identified through extensive comparison to available structures from the literature (35, 75–99).

***A. flavus* strains responded differently to cell wall stress and antifungal drug resistance but similarly to hypoxia and iron starvation.** Hypoxia impacted growth of all strains negatively, but *A. parasiticus* NRRL 2999 was significantly less impacted than all other strains ($P = 0.0346$). Growth of *A. arachidicola* IC26646 was most impacted by the hypoxic environment, although it did not significantly differ from *A. arachidicola* IC26645 or *A. flavus* NRRL 1957. Responses of *A. parasiticus* strains to hypoxia were significantly different ($P = 0.027$), whereas observed differences between strains of *A. flavus* and between *A. arachidicola* strains were not (Fig. 6A).

Under iron starvation conditions (growth in iron-depleted medium), *A. parasiticus* NRRL 2999 was least impacted and grew slightly better than it did in iron-supplemented medium. Growth of *A. flavus* NRRL 501 was most impacted by the lack of iron (Fig. 6B). *A. flavus* strains differed significantly from *A. parasiticus* strains under iron starvation conditions ($P < 0.0001$, one-way analysis of variance [ANOVA]) and from one another ($P = 0.0398$). Growth differences of the two *A. parasiticus* strains under iron starvation conditions were

TABLE 3 Variation in the presence or absence of secondary metabolites in the seven strains from four *Aspergillus* species[a]

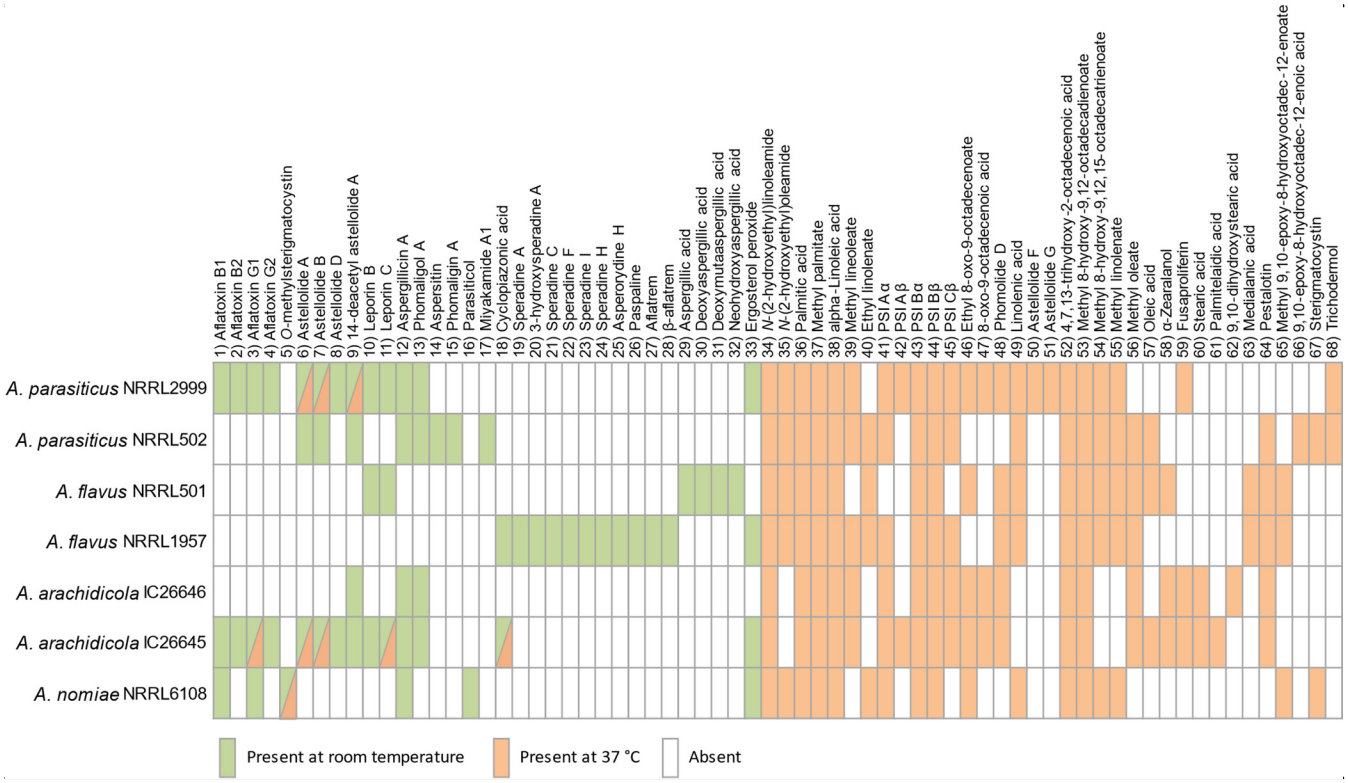

[a]Green indicates metabolites produced at room temperature, and orange indicates metabolites produced at 37°C.

also statistically significant ($P = 0.0030$), as were dissimilarities in growth rates of the two *A. arachidicola* strains ($P < 0.0001$). *A. flavus* NRRL 1957 was more sensitive to oxidative stress than the other strains ($P = 0.0003$).

Strains of *A. flavus* had varied responses to cell wall stress, with a stronger impact of Congo red on the growth of NRRL 501 than that of NRRL 1957 ($P < 0.0001$, two-way ANOVA). *A. flavus* NRRL 501 was significantly more sensitive to cell wall stress than any other strain ($P < 0.0001$). *A. parasiticus* strains also exhibited different growth rates in the presence of Congo red, with NRRL 2999 growing less than NRRL 502 ($P < 0.0001$). Growth of the two *A. arachidicola* strains was not significantly different between the two or from *A. flavus* NRRL 1957 for either concentration of Congo red (Fig. 6C).

Aspergillus parasiticus NRRL2999 had the lowest MIC of amphotericin B (0.5 μg/mL), with all other strains requiring a higher dose to inhibit growth (1 μg/mL). Both *A. arachidicola* strains and *A. nomiae* NRRL 6108 had a higher MIC of voriconazole, with *A. parasiticus* and *A. flavus* strains being more susceptible (Table 4).

***A. flavus* is not significantly more virulent than related, nonpathogenic species in an invertebrate model of fungal disease.** Using an invertebrate model of fungal disease, we evaluated virulence for all strains. *A. fumigatus* virulence assays typically use concentrations of 1×10^6 conidia (asexual spores) to inoculate *Galleria mellonella* larvae (41, 42). When we inoculated larvae with section *Flavi* species at 1×10^6, all animals died within 2 days. Previous studies provided evidence that *A. flavus* kills *G. mellonella* larvae faster than *A. fumigatus* and therefore requires a lower inoculum (100). At a lower concentration of inoculum, 1×10^4 conidia (spores), the larvae survived longer and differences among strains were apparent.

We found that strains of the same species varied widely in their virulence profiles and that strains of the pathogen *A. flavus* were not more virulent than strains of the nonpathogenic species (Fig. 7). Using a 1×10^4 concentration of spores, *A. parasiticus* NRRL 2999 killed the fewest animals and was not statistically different from the

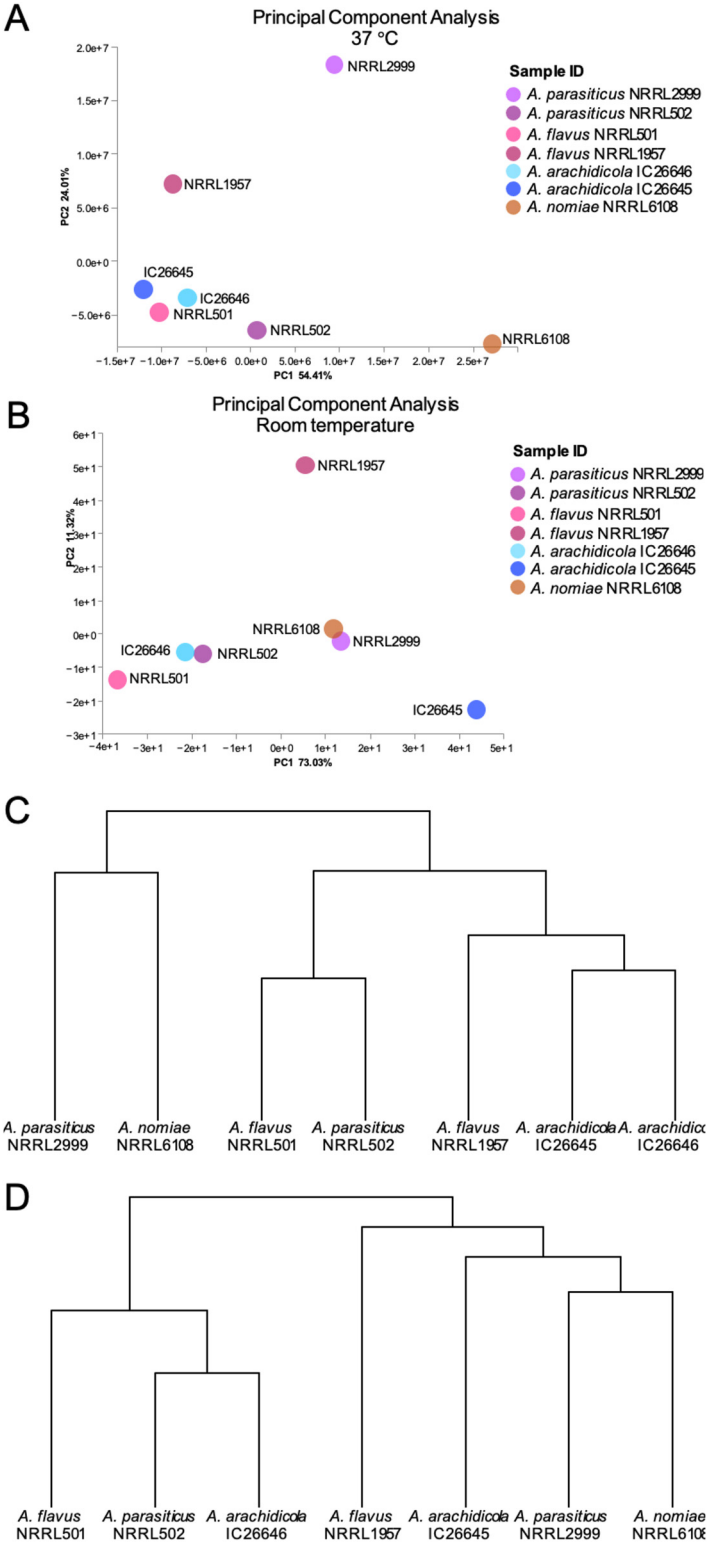

FIG 5 The metabolic profiles of *Aspergillus flavus* strains were more similar at 37°C than room temperature. The metabolomic profiles of *A. flavus* NRRL 501 and NRRL 1957 were almost identical at 37°C, showing very similar metabolites in the UPLC-MS analysis; most of the metabolites identified were fatty acids and ergosterol derivatives. In contrast, the profiles were significantly different at room temperature. (A) Principal-component analysis for all strains at 37°C. Circles represent both presence of metabolites and relative abundance. (B) Principal-component analysis for all strains at room temperature. Circles represent both presence of metabolites and relative abundance. (C) Hierarchical clustering of strains based on metabolite profiles at 37°C. (D) Hierarchical clustering of strains based on metabolite profiles at room temperature.

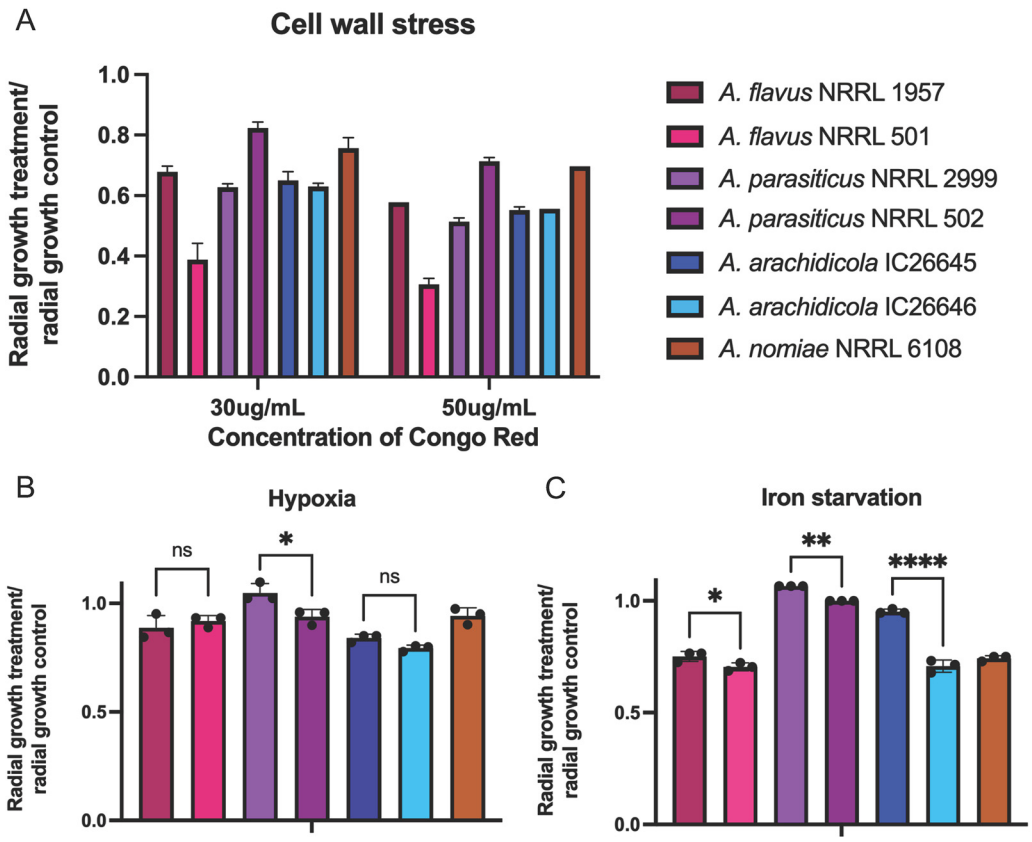

FIG 6 Iron starvation and cell wall stress impacted growth of *A. flavus* strains differently, but hypoxic conditions impacted *A. flavus* strains similarly. For each of the seven *Aspergillus* strains, radial growth is expressed as a ratio of colony radial diameter (in centimeters) of growth under the stress condition divided by the colony radial diameter in the control (solid minimal medium). Not all significant comparisons are shown. (A) Hypoxic stress was induced by incubating plates in 1% O_2 and 5% CO_2. Statistical significance of growth differences among species was primarily driven by growth of *A. parasiticus* NRRL 2999, which was significantly less impacted by hypoxia than other strains. (B) Iron starvation was induced through growth on iron-depleted substrate in the presence of gallium. All species with multiple strains exhibited strain heterogeneity, and *A. parasiticus* grew significantly better under iron starvation conditions than other species. Other species comparisons between species were nonsignificant. (C) Cell wall perturbation was induced by adding Congo red to the medium. *A. flavus* NRRL 501 was most impacted by Congo red at both concentrations, and *A. parasiticus* NRRL 502 was impacted the least. At both concentrations, strains of *A. flavus* had significantly different responses to cell wall stress ($P < 0.0001$). Cell wall stress also impacted *A. parasiticus* strains differently ($P < 0.0001$). Strains of *A. arachidicola* did not have significant growth differences. ns, not significant; *, $P \leq 0.05$; **, $P < 0.005$; ***, $P < 0.0005$ (ANOVA).

phosphate-buffered saline (PBS) control injections. In contrast, *A. arachidicola* IC26646, *A. flavus* NRRL 1957, and *A. parasiticus* 501 killed all inoculated moth larvae by day 3. Of note, the three most virulent strains were all from different species, as were the three least virulent strains; strains of the same species killed larvae at significantly different rates (Fig. 7).

Section *Flavi* strains infected eyes as well as *A. fumigatus* in a murine model of fungal keratitis. Finally, we used a mouse model of keratitis to compare one strain from each of the four different *Aspergillus* species at 24, 48, and 72 h postinfection (Fig. 8A). We included *A. fumigatus* Af293 along with the three section *Flavi* species (*A. arachidicola* IC26646, *A. flavus* NRRL 1957, and *A. parasiticus* NRRL 2999) to benchmark the virulence of section *Flavi* species against the reference strain for section *Fumigati*. We observed significantly lower disease severity (Fig. 8B) and corneal thickness (Fig. 8C) in *A. arachidicola* IC26646 infections compared to the those with other species at 48 h postinfection, but this difference was not significant at 72 h. Fungal burden was not significantly different between the four species (Fig. 8D).

DISCUSSION

With the goal of studying the evolution of pathogenicity in section *Flavi*, we examined the genomes, chemotypes, and phenotypes of four closely related species: the

TABLE 4 MICs of the antifungal drugs amphotericin B and voriconazole for the seven strains of four *Aspergillus* species

	MIC (μg/mL)	
Strain	**Amphotericin B**	**Voriconazole**
Aspergillus arachidicola IC26645	1.0	1.0
Aspergillus arachidicola IC26646	1.0	1.0
Aspergillus flavus NRRL1957	1.0	0.5
Aspergillus flavus NRRL 501	1.0	0.5
Aspergillus nomiae NRRL 6108	1.0	1.0
Aspergillus parasiticus NRRL 502	1.0	0.5
Aspergillus parasiticus NRRL 2999	0.5	0.5

major pathogen *A. flavus* and three related nonpathogenic species, *A. arachidicola*, *A. parasiticus*, and *A. nomiae*. We observed similarities and differences between *A. flavus* and the three nonpathogenic relatives, including shared gene content, variable production of secondary metabolites, and virulence in two animal disease models.

Genomic content was highly similar between strains of the same species, with few strain-specific protein families identified. Predicted BGCs were similar between strains of the same species, with 21 shared by all strains. Georgianna et al. (101) previously predicted 55 BGCs from *A. flavus* NRRL 3357. Of these, 14 BGCs have been linked to a specific metabolite. Additional clusters producing kojic acid, aflavinines, apseripin-2a, and ustiloxins were later identified. Recently, Drott et al. (102) studied 94 different *A. flavus* strains and identified 92 unique BGCs. Our *A. flavus* strains were predicted to contain 70 to 71 BGCs, well within the expected range, although over half of the predicted BGCs in each strain have not been linked to known metabolites. Our results of the number and type of predicted BGCs per strain are in line with results from Kjærbølling et al. (31), who also found that *A. parasiticus* had more predicted biosynthetic backbone genes than *A. arachidicola*, *A. flavus*, or *A. nomiae*. However, the *A. nomiae* strain studied by Kjærbølling et al. (NRRL 13137) was predicted to encode more backbone genes than our strain (NRRL 6108), further highlighting strain-level differences within species.

Among the species with multiple strains included, the two *A. parasiticus* strains shared the fewest species-specific protein families (1,230), whereas pairs of strains from *A. arachidicola* and *A. flavus* shared over 3,000 species-specific protein families between strains, around 20% of the total number of protein families for each species. Our results within section *Flavi* contrast with observations within section *Fumigati*, which show a lower proportion of species-specific genes for *A. fumigatus* than in related, nonpathogenic species (103). Specifically, when strains of *A. fumigatus* were compared to other section *Fumigati* species, only 72 families were identified as unique to *A. fumigatus* (103); in contrast, we observed over 1,000 unique families in *A. flavus*. Although section *Flavi* species are known to have larger genomes and encode more predicted proteins than *A. fumigatus* (31), this does not explain the huge difference in number of species-specific protein families between *A. fumigatus* and *A. flavus* and further emphasizes that the two sections are quite distinct in their genomic compositions.

Resistance to antifungal drugs was also similar between strains of the same species and within previously reported ranges for *A. flavus* (104). Our *A. flavus* and *A. parasiticus* strains were more susceptible to amphotericin B than clinical strains of the same species from Brazil (105), and strains from all four species had similar susceptibility to voriconazole as clinical strains from Brazil (106, 107). As expected, our *Flavi* strains were generally more resistant to amphotericin B than to voriconazole.

Several traits that we examined revealed heterogeneity between strains of the same species, indicating diversity within each species as well as among species. Our two *A. flavus* strains, NRRL 501 and NRRL 1957, for example, did not produce any of the same secondary metabolites when grown at room temperature, and only a handful of

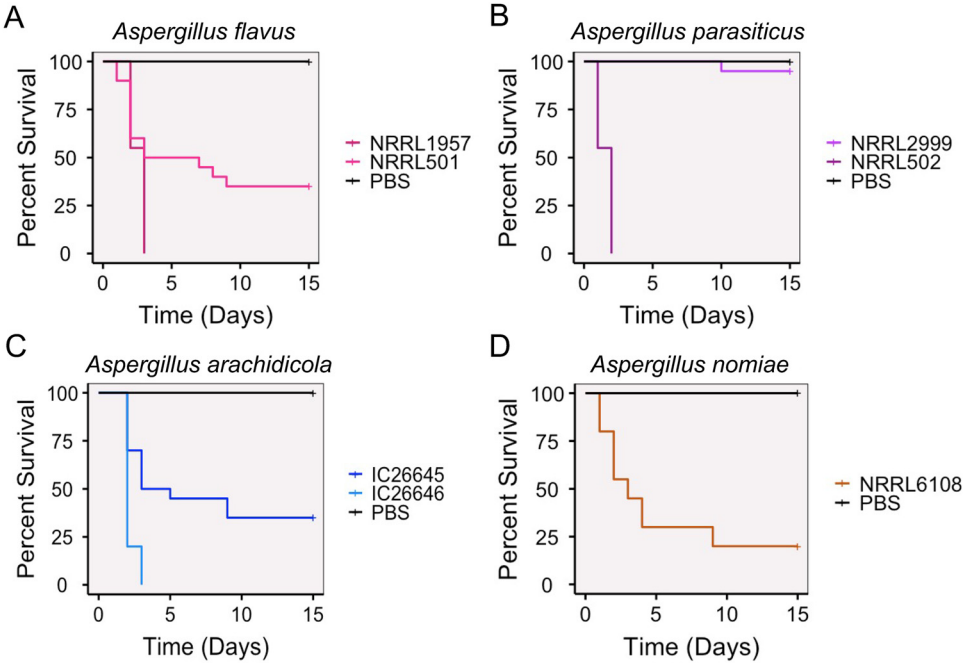

FIG 7 *Aspergillus flavus* was not significantly more virulent than related nonpathogenic species in an invertebrate model of fungal disease. Cumulative survival of *Galleria mellonella* larvae inoculated with 1×10^4 asexual spores (conidia) of an *Aspergillus* strain or a PBS control. (A) Survival for larvae inoculated with either *A. flavus* NRRL 1957 or NRRL 501. All pairwise comparisons between the two strains and the control group were statistically significant. (B) Survival for larvae inoculated with either *A. parasiticus* NRRL 2999 or NRRL 502. *A. parasiticus* NRRL 2999 was not statistically different from the control group, but NRRL 502 was statistically different from both the control and NRRL 2999. (C) Survival for larvae inoculated with either *A. arachidicola* IC26645 or IC26646. All pairwise comparisons between the two strains and the control group were statistically significant. (D) Survival for larvae inoculated with *A. nomiae* NRRL 6108. Survival of NRRL 6108 was statistically different from the control survival.

compounds produced by the two strains at room temperatures overlapped with those produced by strains of other species. We found that our *A. parasiticus* strains produced aflatoxin at higher levels than other species, including noted aflatoxin producer *A. parasiticus* NRRL 2999, although one strain of *A. flavus*, NRRL 1957, had previously been characterized as negative for aflatoxin (107). At the temperature of the human body, which better models infection-relevant conditions, several compounds were produced by all seven strains. These included fatty acids such as palmitic acid, which has been implicated in inflammation (108), and precocious sexual inducer factors. Interestingly, our two *A. flavus* strains had highly similar chemical profiles at 37°C.

Strains of the same species also responded differently to environmental stressors in growth assays, including cell wall stress and iron starvation, which may affect a strain's fitness within a human host. For example, the ability to tolerate cell wall stress (induced by Congo red) correlated with higher virulence in an invertebrate model, as observed in *A. flavus* NRRL 1957 and *A. parasiticus* NRRL 502. Genetic determinants of virulence in *A. flavus*, including those involved in cell wall integrity, stress response, and transcription, were found in all strains. Virulence-associated genes involved in secondary metabolism were missing in *A. flavus* NRRL 501 as a result of the aflatoxin biosynthetic gene cluster absence in the strain. Several genetic determinants of virulence within *A. flavus* influence aflatoxin production as well as conidiation and fungal development (43, 47, 52, 56, 58), with multiple genes within the pathway itself directly implicated in virulence (69, 72), indicating aflatoxin production is intertwined with basic biological functions of the fungus. Therefore, aflatoxin production may also impact pathogenicity in animals, although few studies include animal models and current study of virulence within *A. flavus* is dominated by seed inoculation assays and spore counts that are of relevance to its role in plant disease. However, knockout mutants of some genes have been shown to decrease virulence in both plant and

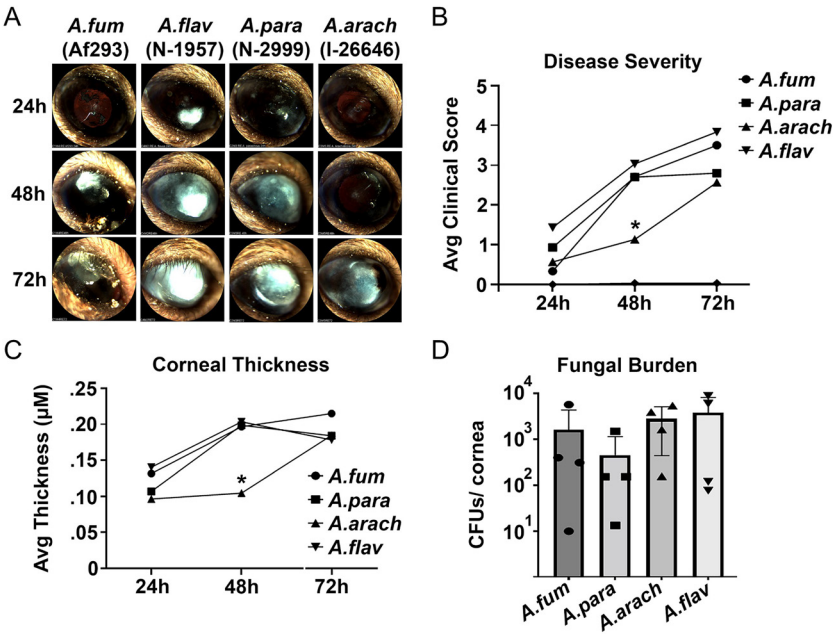

FIG 8 Section *Flavi* species infected eyes as well as *A. fumigatus* did in a murine model. (A) Slit-lamp images of a representative animal for each infection group. (B) Clinical score analysis of all slit-lamp images revealed reduced disease severity in the *A. arachidicola* group at 48 h postinfection (n = 5/group). (C) Corneal thickness measured by optical coherence tomography similarly revealed reduced structural alteration in the *A. arachidicola* group at 48 h (n = 5). (D) CFU analysis on resected corneas revealed indistinguishable fungal burden at 72 h postinfection between infection groups. *A.arach*, *A. arachidicola* IC26646; *A.flav*, *A. flavus* NRRL 1957; *A.fum*, *A. fumigatus* Af293; *A.para*, *A. parasiticus* NRRL 2999.

animal models of infection (42), demonstrating parallels between the plant pathogenesis and animal pathogenesis, a phenomenon also seen in other opportunistic fungal pathogens (109).

Surprisingly, in *Galleria mellonella*, neither *A. flavus* strain was the most virulent, and all species were able to infect and kill at least some larvae, although *A. parasiticus* NRRL 2999 killed only 10% of larvae. As observed previously, the concentration of asexual spores required to kill all larvae within 24 h was orders of magnitude lower for infection with section *Flavi* species compared to section *Fumigati* species (110), suggesting higher virulence in the section *Flavi* species. In the most virulent section *Flavi* strains (*A. parasiticus* NRRL502, *A. flavus* NRRL1957, and *A. arachidicola* IC26646), death of all larvae occurred within 72 h. A previous study using a lower concentration inoculum (1×10^3 spores) saw 100% mortality of larvae in the first 48 h for *Galleria* infected with *A. flavus* (110). However, in another study of *A. flavus* strains, also with a concentration of 1×10^3 spores, 10% or more of the larvae were alive after 72 h for all strains (111). Few studies of non-*A. flavus* section *Flavi* species have included virulence assays in *Galleria*, presumably due to their status as nonpathogenic, but this prevents direct comparison between our results and previous studies for species other than *A. flavus*. As a known entomopathogen (112), virulence by *A. flavus* in an invertebrate model may be correlated with insecticidal traits rather than (or in addition to) human pathogenicity.

To examine virulence in a mammalian model of fungal keratitis, we infected eyes of mice with one strain each of *A. flavus*, *A. arachidicola*, and *A. parasiticus*, along with one *A. fumigatus* strain. We observed faster colonization of mice by *A. flavus* than *A. fumigatus* at 24 h, although fungal burden and disease severity were consistent for all species by 72 h. *A. arachidicola* IC26646 did not infect as quickly, with significantly lower disease severity observed at 48 h postinfection, but the level caught up to the others by 72 h postinfection. Mouse models of disease are a useful tool for understanding disease progression and characterizing differences among strains, but previous studies

have induced systemic infections leading to mouse death (113). Systemic infection studies have shown *A. flavus* to be more virulent than *A. fumigatus* (24, 113), despite higher rates of aspergillosis caused by *A. fumigatus*. Interestingly, we observed no difference in disease severity at 72 h between the two species in our keratitis model. The similarity of secondary metabolite profiles for strains at 37°C, coupled with the ability of all species to establish infections in both the *Galleria* and murine models, leads us to believe that infection may be more highly dependent on the characteristics of the individual strain rather than species, as observed in other pathogens among *Aspergillus* (114). We intend to compare additional strains of both *A. flavus* and *A. fumigatus*, including patient-derived clinical strains, to examine differences in virulence and disease progression of *A. flavus* and *A. fumigatus* in our keratitis model. It remains an open question whether patient-derived clinical strains of *A. flavus* differ from the environmental strains available from culture collections, such as the two strains included in this study, and we hope to explore this dimension of pathogenicity in future studies.

In summary, by examining genomic, chemical, and phenotypic variation within and between closely related pathogenic and nonpathogenic *Aspergillus* section *Flavi* species, we showed that species previously considered nonpathogenic infect at the same rate as the pathogen *A. flavus* in both invertebrate and murine models of disease and, in the case of *A. parasiticus* NRRL 2999, showed that a single strain may be considered avirulent in one model and virulent in another. Therefore, we advocate for the use of multiple disease models for the future study of fungal disease caused by species within section *Flavi*. Our results indicate that strain-level differences may play a major role in infection. Additionally, we showed that predicted biosynthetic gene clusters and genetic determinants of virulence do not differ substantially between strains and therefore do not explain the differences in virulence, possibly implicating as-yet-uncharacterized variations in gene presence or absence between strains and species and/or transcriptomic or posttranslational regulatory mechanisms in the occurrence and prevalence of human disease caused by *Aspergillus* species, particularly *A. flavus*.

MATERIALS AND METHODS

Genome sequencing and comparisons. (i) Strains and growth conditions. Seven strains from four *Aspergillus* species were obtained from the USDA Agricultural Research Service Culture Collection (*A. flavus* NRRL 501, *Aspergillus nomiae* NRRL 6108, and *Aspergillus parasiticus* NRRL 2999) or from the laboratory of Ignazio Carbone at North Carolina State University (*Aspergillus flavus* NRRL 1957, *Aspergillus parasiticus* NRRL 502, and *Aspergillus arachidicola* IC26645 and IC26646). All strains were maintained on potato dextrose agar (PDA; Difco) at room temperature (approximately 23°C).

(ii) Genomic DNA extraction and sequencing. For genomic DNA extraction to facilitate genome sequencing, the strains were first grown on PDA. Each strain was subsequently transferred to a 100-mm petri dish with an overlay of sterile autoclaved Hybond nylon membranes (84 mm) obtained from Amersham (GE Healthcare). The strains were then allowed to grow for 2 to 3 weeks on PDA medium overlaid with this membrane. After suitable growth was achieved, a sterile scalpel was used to harvest the fungal mycelia by scraping the surface of the nylon membrane without dislodging any agar from the petri plate. Using a sterile mortar and pestle, the mycelia were then ground to a fine powder with liquid nitrogen and transferred to a bashing bead tube with 750 μL of DNA lysis buffer (Zymo Quick-DNA fungal/bacterial miniprep kit). The powder in the bashing bead tube was further disrupted and homogenized in a Qiagen tissue lyser LT bead mill for 5 min. Genomic DNA was obtained using the standard protocol for the Zymo Quick-DNA fungal/bacterial miniprep kit.

Paired-end sequencing (2 $\times$ 150 bp) of the genomic DNA was performed at the Vanderbilt Technologies for Advanced Genomics (VANTAGE) facility using the NovaSeq 6000 platform (Illumina, Inc.) following the manufacturer's protocols. Libraries were prepared using the Illumina TruSeq DNA PCR-free kit.

(iii) Genome assembly, annotation, and assessment. Adaptors were removed from the reads and filtered for quality using Trimmomatic v0.39 (115). Trimmed reads were assembled into draft genomes using SPAdes v3.12.0 (116) with the "–careful" flag. Scaffolds under 500 bp were removed from further analysis. Draft genomes were annotated using Liftoff v1.2.0 (117), a sequence-similarity method which requires a reference annotation. *A. flavus* strains and *A. nomiae* NRRL 6108 were annotated using strain NRRL 3357 (118); for *A. arachidicola* strains we used CBS 117612 (31); *A. parasiticus* strains were annotated from CBS 117618 (31). The *A. parasiticus* NRRL 2999 draft genome was compared to that of *A. parasiticus* SU-1 to confirm isolate identity using fastANI (119), which compares average nucleotide identity (ANI) between genomes. Genome and annotation completeness was evaluated using BUSCO v4.0.4 (120), against the eurotiales database of universal single-copy orthologs.

(iv) Phylogenetics. In addition to the 7 newly sequenced genomes, the genomes and predicted proteomes of 23 other *Aspergillus* strains were downloaded from NCBI (Table 5). In total, we used 29

TABLE 5 Genomes of 27 *Aspergillus* strains from 20 species, including 7 newly sequenced genomes[a]

Species	Strain	Reference	Environmental source
Aspergillus alliaceus	CBS 536.65^T	Kjærbølling et al., 2020	Dead blister beetle, Washington, DC, USA
Aspergillus arachidicola	CBS 117610^T	Kjærbølling et al., 2020	
Aspergillus arachidicola	CBS 117612	Kjærbølling et al., 2020	
Aspergillus arachidicola	IC26645 (IBT 27218)	This study	Unknown
Aspergillus arachidicola	IC26646 (IBT 27178; CBS 117615)	This study	*Arachis glabrata* leaf, Argentina
Aspergillus avenaceus	IBT 18842	Kjærbølling et al., 2020	Unknown
Aspergillus bertholletius	IBT 29228	Kjærbølling et al., 2020	
Aspergillus luteovirescens	NRRL 26010^T (CBS 117187)	Kjærbølling et al., 2020	Frass in a silkworm rearing house, Japan
Aspergillus caelatus	CBS 763.97^T	Kjærbølling et al., 2020	Peanut field, GA, USA
Aspergillus coremiiformis	CBS 553.77^T	Kjærbølling et al., 2020	Unknown
Aspergillus flavus	CBS 121.62	Kjærbølling et al., 2020	Unknown
Aspergillus flavus	NRRL 501	This study	Unknown
Aspergillus flavus	NRRL 1957^T (CBS 100927)	This study	Cellophane diaphragm of optical mask, South Pacific
Aspergillus flavus	NRRL 3357	Nierman et al., 2005	Moldy peanuts
Aspergillus leporis	CBS 151.66^T	Kjærbølling et al., 2020	Dung of *Lepus townsendii*, WY, USA
Aspergillus minisclerotigenes	CBS 117635^T	Kjærbølling et al., 2020	*Arachis hypogaea* seed, Argentina
Aspergillus niger (outgroup – section *Nigri*)	CBS 513.88	Pel et al., 2007	
Aspergillus nomiae	NRRL 13137	Moore et al., 2015	Wheat, IL, USA
Aspergillus nomiae	NRRL 6108	This study	Moldy wheat
Aspergillus novoparasiticus	CBS 126849	Kjærbølling et al., 2020	
Aspergillus parasiticus	NRRL 502^T (CBS 100926)	This study	Mealybug on sugar cane, HI, USA
Aspergillus parasiticus	NRRL 2999	This study	Peanuts, Uganda
Aspergillus parasiticus	SU-1	Linz et al., 2014	Peanuts, Uganda
Aspergillus parasiticus	CBS 117618	Kjærbølling et al., 2020	
Aspergillus pseudocaelatus	CBS 117616	Kjærbølling et al., 2020	*Arachis hypogaea*, Nigeria
Aspergillus pseudonomiae	CBS 119388 (NRRL 3353)	Kjærbølling et al., 2020	Diseased alkali bees, USA
Aspergillus pseudotamarii	CBS 117625	Kjærbølling et al., 2020	
Aspergillus sergii	CBS 130017	Kjærbølling et al., 2020	
Aspergillus tamarii	CBS 117626	Kjærbølling et al., 2020	
Aspergillus transmontanensis	CBS 130015	Kjærbølling et al., 2020	

[a]CBS, CBS-KNAW Fungal Biodiversity Centre, Utrecht, the Netherlands; IBT, IBT Culture Collection of Fungi, Lyngby, Denmark; NRRL, USDA-ARS Culture Collection, Peoria, IL, USA.

strains from 18 species of section *Flavi* to build a species tree phylogeny of *Aspergillus* section *Flavi*, with *Aspergillus niger* CBS 513.88 (section *Nigri*) serving as an outgroup. Single-copy orthologous proteins in all 30 strains were identified using OrthoFinder v2.5.4 (121). For each ortholog, all 30 copies were aligned using Muscle v3.8.1551 (122), and the amino acid alignments were trimmed using trimAl v1.2 (123) with the gappyout option. Alignments shorter than 200 amino acids were removed from analysis, and the remaining alignments were concatenated into a single data matrix using the script catfasta2phyml.pl (https://github.com/nylander/catfasta2phyml). A maximum likelihood phylogeny was reconstructed using IQ-tree v1.6.1 (124) with the JTT+F+I+G4 model and 1,000 replicates for bootstrapping. The resulting consensus tree was viewed using iTOL (125).

(v) Identification of orthologous and unique protein families and biosynthetic gene clusters. Using the seven newly sequenced strains (*A. flavus* NRRL 501 and NRRL 1957, *A. parasiticus* NRRL 502 and NRRL 2999, *A. nomiae* NRRL 6108, and *A. arachidicola* IC26645 and IC26646), we compared each predicted proteome in a pairwise manner and in combination to identify unique and orthologous proteins for all combinations using OrthoVenn2 (126). Within the unique or orthologous protein groups, enriched GO categories were identified from UniProt annotations (127), and probability testing was based on hypergeometric distribution (126). The R package UpSetR was used to visualize the number of shared protein families in each grouping as an upset plot. BGCs were predicted using fungiSMASH v6.0 (128). BGCs from different strains were compared using BiGSCAPE-CORASON (129) with a cutoff set to 0.70, and BGCs shared between all strains and strains of the same species were identified. Synteny plots of BGCs of interest were visualized using Clinker (130).

Secondary metabolite isolation and structural elucidation. The profile of secondary metabolites for the seven *Aspergillus* section *Flavi* strains were investigated using well-established procedures (26). Each strain was grown at both 23°C (i.e., room temperature) and 37°C on oatmeal (Quaker Oats old-fashioned breakfast oats). Since the lacrimal fluid was composed of physiologic saline, the oatmeal cultures were prepared both with and without 6 mg/mL saline to assess if saline impacted the profile of secondary metabolites.

Solid-state fermentations (n = 6) were carried out in broad-mouthed 250-mL Erlenmeyer flasks. To start oatmeal cultures, an agar plug from the leading edge of a PDA petri dish culture was transferred to a sterile tube with 10 mL of liquid yeast extract-soy-dextrose (YESD; 20 g soy peptone, 20 g dextrose, 5 g yeast extract,

in 1 liter distilled H_2O) and grown for 7 days on an orbital shaker (100 rpm) at room temperature (~23°C), and then used to inoculate the oatmeal solid fermentation medium. Oatmeal cereal medium (Quaker Oats) was prepared by adding 10 g oatmeal to a 250-mL Erlenmeyer flask with either 15 to 17 mL of deionized H_2O (DI-H_2O) or 15 to 17 mL of a 6-mg/mL saline solution (i.e., 6 g of Instant Ocean in 1,000 mL of DI-H_2O) and then autoclaving at 121°C for 30 min. For each of the seven strains, six fermentation flasks were incubated at room temperature with saline and six without saline; similarly, six flasks were incubated at 37°C with saline and six without saline. Therefore, for each strain, 24 Erlenmeyer flasks were grown in total. Prior to analysis of the secondary metabolite profiles, the cultures were incubated statically at room temperature for 14 days or 37°C for 7 days.

(i) Extraction of secondary metabolites. For each condition, each of the six culture flasks was extracted individually and treated as a biological replicate. Each individual flask was extracted by adding 60 mL of $CHCl_3$-methanol (MeOH; 1:1), chopping with a spatula, and shaking overnight (~16 h) at 100 rpm at room temperature. The cultures were then filtered *in vacuo*, and 90 mL of $CHCl_3$ and 150 mL of DI-H_2O were added to each of the filtrates. The mixtures were then transferred to a separatory funnel and shaken vigorously. The organic layer (i.e., bottom layer) was drawn off and evaporated to dryness *in vacuo*. The dried organic layer was reconstituted in a 100-mL mixture of CH_3CN-MeOH (1:1) and 100 mL of hexanes, transferred to a separatory funnel, and shaken vigorously. The defatted organic layers (i.e., CH_3CN-MeOH layers) were evaporated to dryness.

All the defatted organic layers were analyzed individually by ultraperformance liquid chromatography–high-resolution mass spectrometry (UPLC-HRMS), utilizing a Thermo LTQ Orbitrap XL mass spectrometer equipped with an electrospray ionization source. A Waters Acquity UPLC was utilized with a BEH C_{18} column (1.7 μm; 50 mm × 2.1 mm) set to a temperature of 40°C and a flow rate of 0.3 mL/min. The mobile phase consisted of a linear gradient of CH_3CN-H_2O (both acidified with 0.1% formic acid), starting at 15% CH_3CN and increasing linearly to 100% CH_3CN over 8 min, with a 1.5-min hold before returning to the starting conditions.

(ii) Metabolomic analysis. PCA and hierarchical clustering were performed on the UPLC-HRMS data. Untargeted UPLC-HRMS data sets for each sample were individually aligned, filtered, and analyzed using Mzmine 2.53 software (https://sourceforge.net/projects/mzmine/). Peak list filtering and retention time alignment algorithms were used to refine peak detection, and the join algorithm integrated all sample profiles into a data matrix using the following parameters: mass detection (MS1 level, centroid positive mode); ADAP chromatogram builder (group intensity threshold, 20,000; minimum highest intensity, 60,000; *m/z* tolerance, 0.003); chromatogram deconvolution (wavelets (ADAP) algorithm). For join aligner and gap filling the following parameters were used: retention time tolerance, 0.05 min; *m/z* tolerance, 0.0015 *m/z*. The resulting data matrix was exported to Excel (Microsoft) for analysis as a set of *m/z*-retention time (RT) pairs with individual peak areas. Samples that did not possess detectable quantities of a given marker ion were assigned a peak area of zero to maintain the same number of variables for all sample sets. Ions that did not elute between 1 and 10 min and/or had an *m/z* ratio of $<$200 or $>$900 Da were removed from analysis. Relative standard deviation was used to understand the quantity of variance between the injections, which may have differed slightly based on instrument variance. A cutoff of 1.0 was used at any given *m/z*-RT pair across the biological replicate injections, and if the variance was greater than the cutoff, it was assigned a peak area of zero. PCA and hierarchical clustering were conducted with Python. The PCA score plots were generated using the averaged data of the six individual biological replicates.

(iii) Isolation and identification of secondary metabolites. After comparison of the UPLC-HRMS data, the defatted organic layers for each condition were combined due to the similarity of their chemical profiles, so as to generate a larger pool of material for isolation studies, which were carried out using well-established natural products chemistry procedures (131, 132). The fractions were dissolved in $CHCl_3$-MeOH, absorbed onto Celite 545 (Acros Organics), and fractioned by normal-phase flash chromatography using a gradient of hexane-$CHCl_3$-MeOH. The isolation of the compounds was carried out using preparative high-performance LC (HPLC).

The isolated fungal metabolites were identified by direct comparison of the spectroscopic and spectrometric properties with those previously reported, and where possible, structures were validated by comparisons with authentic reference standards (133). Additionally, mass defect filtering (134) was used to identify structurally related analogs of the isolated compounds.

(iv) General experimental procedures. The nuclear magnetic resonance (NMR) data were collected using a JEOL ECS-500 spectrometer operating at 500 MHz for ^1H and at 125 MHz for ^{13}C, or an Agilent 700-MHz spectrometer, equipped with a cryoprobe, operating at 700 MHz for ^1H and at 175 MHz for ^{13}C. The HPLC separations were performed on a Varian Prostar HPLC system equipped with a Prostar 210 pump and a Prostar 335 photodiode array detector, with the collection and analysis of data using Galaxy Chromatography Workstation software. The columns used for separations were either a Synergi C_{18} preparative column (4 μm; 21.2 × 250 mm) at a flow rate of 21.2 mL/min, a Luna PFP(2) preparative column (5 μm; 21.2 × 250 mm) at a flow rate of 17 mL/min, or an Atlantis T3 C_{18} preparative column (5 μm; 19 × 250 mm) at a flow rate of 17 mL/min. Flash chromatography was performed on a Teledyne ISCO Combiflash Rf 200 as monitored by evaporative light-scattering and photodiode array detectors.

Growth assays. (i) Antifungal drug susceptibility testing. Antifungal susceptibility testing for both voriconazole (Sigma-Aldrich) and amphotericin B (Sigma-Aldrich) was performed by determining the MIC according to the protocol established by the Clinical and Laboratory Standards Institute.

(ii) Stress response. Radial growth was used to compare how the different strains responded to cell wall stress, iron starvation, and hypoxia. Strains were grown in solid minimal medium (MM), as described previously (135), inoculated with 1×10^5 spores of each strain, and incubated for 5 days at 37°C before

colony diameter was measured. To induce cell wall stress, 30 or 50 μg/mL of Congo red (cell wall perturbing) was added to the medium. For iron starvation, iron-poor MM was devoid of all iron and supplemented with 128 μg/mL of gallium nitrate (Sigma-Aldrich). Gallium is chemically similar to iron, and for this reason it is taken up by the cell to replace iron (136). Radial growth for the aforementioned stresses was expressed as a ratio, dividing colony radial diameter (in centimeters) of growth under the stress condition by the colony radial diameter in the control (no-stress) condition. For hypoxia analysis, the plates were incubated on 5% CO_2 and 1% O_2 at 37°C for 5 days.

Oxidative stress was measured using the protocol described by Canóvas et al. (137). Briefly, the experiments were performed in 96-well plates containing 100 μL of MM (with 1% agar) supplemented or not with 3 mM H_2O_2 (Merck S.A.) or 0.15 mM menadione (Sigma-Aldrich). Each well was inoculated with 1×10^5 spores, and the growth was measured over time by quantifying the absorbance at 595 nm in a plate reader (Synergy HT) at 37°C. Data were recorded and analyzed with Gen5 data analysis software v2.0 and exported to Microsoft Excel for further analysis and generation of the graphs. Lag times were calculated using Gen5 data analysis software v2.0 as the time interval between the line of maximum slope of the propagation phase and the absorbance baseline at time zero.

(iii) Statistical evaluation of growth assay results. A one-way ANOVA was calculated for the iron starvation, hypoxia, and oxidative stress data sets, and a two-way ANOVA was calculated for the data set of cell wall stress with two Congo red concentrations. Graphs were visualized and statistics were calculated using GraphPad Prism v9.3.1.

Assessment of virulence using an invertebrate model of fungal disease, *Galleria mellonella*. (i) Preparation of larvae and inoculum. *Galleria mellonella* larvae were used to investigate the virulence of all seven strains. The larvae used for the infection were in the last larval stage of development (sixth week). All selected larvae weighed ~300 mg and were restricted to food for 24 h before the experiment. Fresh asexual spores (conidia) of each strain were counted using a hemocytometer.

(ii) Inoculation and observation. Five microliters of each inoculum was injected using a Hamilton syringe (model 7000.5 KH) through the last left ear (n = 10/group), resulting in 1×10^6, 1×10^4, and 1×10^3 conidia/larva. The control group was inoculated with PBS. After infection, the larvae were kept with food restrictions at 37°C in petri dishes in the dark and scored daily for 15 days. The larvae were considered dead based on a lack of movement in response to touch. The viability of the inoculum administered was determined by serial dilution of the conidia in yeast extract-agar-glucose medium and incubating the plates at 37°C for 72 h. The experiment was repeated twice.

We separated and assembled the groups with the larvae (n = 10) in petri dishes. The groups were composed of larvae that were approximately 300 mg in weight and 2 cm long. Moth sex was not accounted for due to the impossibility of visually determining sex at the sixth week of larval development.

(iii) Statistical analysis of infection rates. Larval survival was plotted on Kaplan-Meier curves using the survival and survminer R packages. A Mantel-Cox log-rank test was used to evaluate statistical significance between the survival curves of larvae infected with different fungal strains.

Assessment of virulence using a murine model of keratitis. (i) Preparation of fungal inoculum. On the day of corneal inoculation, asexual spores (conidia) of *A. arachidicola* IC26646, *A. flavus* NRRL 1957, *A. fumigatus* Af293, and *A. parasiticus* NRRL 2999 were incubated in 25 mL yeast extract-peptone-dextrose broth at a density of 5×10^6 conidia/mL at 35°C, 200 rpm. Once conidia were swollen and clumping but not polarized (approximately 4 h for all strains), cultures were collected by centrifugation, washed twice with PBS, resuspended in PBS to an optical density of 0.8 (360 nm), and stored at room temperature until the corneal inoculation (approximately 1 h).

(ii) Corneal infections. On the day preceding corneal inoculation, 6- to 8-week-old male C57BL/6J mice (Jackson Laboratories) were immunosuppressed with a 100 mg/kg methylprednisolone by intraperitoneal (i.p.) injection. The following day, animals were anesthetized with 100 mg/kg ketamine and 6.6 mg/kg xylazine, i.p., and the corneal epithelium was ulcerated over the pupil of the right eye to a diameter of ~1 mm by using an Algerbrush II. Five microliters of the fungal inoculum (described above) was pipetted over the ulcerated cornea and remained in place for 20 min before being removed with a Kim wipe. Five animals were included in each infection group, and the contralateral eye of each animal remained uninfected in accordance with the Association for Research in Vision and Ophthalmology guidelines for the use of animals in vision research. Animals were further injected subcutaneously with 1 mg/kg Buprenorphine SR for analgesia.

(iii) Slit-lamp microscopy and disease scoring. Each day postinoculation (p.i.), animals were anesthetized with isoflurane and imaged by slit-lamp using a Micron IV biomicroscope (Phoenix Technology Group, CA, USA). Images were deidentified and assigned an overall disease score (range, 0 to 4) by two blinded reviewers based on the area of opacification, density of opacification, and surface irregularity. The average disease scores for each cornea were compared by one-way ANOVA using GraphPad Prism v9.3.1.

(iv) Optical coherence imaging and corneal thickness measurement. Corneas were also imaged using the Bioptigen spectral domain-optical coherence tomography system (Leica Microsystems, Deerfield, IL, USA). Mice were anesthetized with isoflurane, and a 4- by 4-mm image was scanned with a 12-mm telecentric lens. Reference arm calibration was completed by the manufacturer and set to 885. Images were analyzed using the InVivoVue Diver software (Bioptigen). Briefly, corneal scans were digitally overlaid with a 11 by 11 spiderplot, and the distance between the epithelium and endothelium was measured at 11 distinct points near the central cornea. The average of the 11 measures was taken as the corneal thickness (in millimeters) and compared across groups using a one-way ANOVA in GraphPad Prism v9.3.1.

(v) Fungal burden assessment. At 72 h p.i., corneas were resected and homogenized by incubation in 1 mL of buffer containing 2 mg/mL collagenase I (Sigma) for 1 h at 37°C. Dilutions of the homogenate

were plated onto inhibitory mold agar and incubated overnight at 35°C, and colonies were enumerated. Colony counts were compared between groups using a one-way ANOVA in GraphPad Prism v9.3.1.

Data availability. Sequencing data and genome assemblies associated with this project are compiled under BioProject PRJNA824811. Raw reads are available through the NCBI sequence read archive under accession numbers SRR19347655 (*Aspergillus arachidicola* IC26646), SRR19347656 (*Aspergillus arachidicola* IC26645), SRR19347505 (*Aspergillus flavus* NRRL 1957), SRR18725159 (*Aspergillus flavus* NRRL 501), SRR19347653 (*Aspergillus parasiticus* NRRL 2999), SRR19347654 (*Aspergillus parasiticus* NRRL 502), and SRR19369914 (*Aspergillus nomiae* NRRL 6108).

The NMR data for compounds **1**, **3**, **6**, **12**, **22**, **26** and **57** were deposited in the Natural Products Magnetic Resonance Database and can be accessed at https://npmrd-project.org/.

Supplementary tables and figures are available on FigShare at https://doi.org/10.6084/m9.figshare.20256336.

ACKNOWLEDGMENTS

We thank the Rokas lab, and in particular Matthew Mead, for helpful discussion and feedback. E.A.H. is supported by the National Institutes of Health National Eye Institute (F31 EY033235). Research in A.R.'s lab is supported by grants from the National Science Foundation (DEB-2110404), the National Institutes of Health National Institute of Allergy and Infectious Diseases (R56 AI146096 and R01 AI153356), and the Burroughs Wellcome Fund. The content is solely the responsibility of the authors and does not necessarily represent the official views of the National Institutes of Health. At UNCG, some of the NMR studies were performed in part at the Joint School of Nanoscience and Nanoengineering, a member of the National Nanotechnology Coordinated Infrastructure (NNCI), which is supported by the National Science Foundation (Grant ECCS-2025462).

A.R. is a scientific consultant for LifeMine Therapeutics, Inc., and N.H.O. is a member of the Scientific Advisory Board of Mycosynthetix, Inc.

REFERENCES

1. Anonymous. 2017. Stop neglecting fungi. Nat Microbiol 2:17120. https://doi.org/10.1038/nmicrobiol.2017.120.
2. Bongomin F, Gago S, Oladele RO, Denning DW. 2017. Global and multinational prevalence of fungal diseases—estimate precision. J Fungi 3:57. https://doi.org/10.3390/jof3040057.
3. Cunha C, Aversa F, Romani L, Carvalho A. 2013. Human genetic susceptibility to invasive aspergillosis. PLoS Pathog 9:e1003434. https://doi.org/10.1371/journal.ppat.1003434.
4. Salehi M, Khajavirad N, Seifi A, Salahshour F, Jahanbin B, Kazemizadeh H, Hashemi SJ, Dehghan Manshadi SA, Kord M, Verweij PE, Khodavaisy S. 2021. Proven Aspergillus flavus pulmonary aspergillosis in a COVID-19 patient: a case report and review of the literature. Mycoses 64:809–816. https://doi.org/10.1111/myc.13255.
5. Schauwvlieghe AFAD, Rijnders BJA, Philips N, Verwijs R, Vanderbeke L, Van Tienen C, Lagrou K, Verweij PE, Van de Veerdonk FL, Gommers D, Spronk P, Bergmans DCJJ, Hoedemaekers A, Andrinopoulou E-R, van den Berg CHSB, Juffermans NP, Hodiamont CJ, Vonk AG, Depuydt P, Boelens J, Wauters J. 2018. Invasive aspergillosis in patients admitted to the intensive care unit with severe influenza: a retrospective cohort study. Lancet Respir Med 6:782–792. https://doi.org/10.1016/S2213-2600(18)30274-1.
6. Brown L, Leck AK, Gichangi M, Burton MJ, Denning DW. 2021. The global incidence and diagnosis of fungal keratitis. Lancet Infect Dis 21:e49–e57. https://doi.org/10.1016/S1473-3099(20)30448-5.
7. Thomas PA, Kaliamurthy J. 2013. Mycotic keratitis: epidemiology, diagnosis and management. Clin Microbiol Infect 19:210–220. https://doi.org/10.1111/1469-0691.12126.
8. Al-Hatmi AMS, Castro MA, de Hoog GS, Badali H, Alvarado VF, Verweij PE, Meis JF, Zago VV. 2019. Epidemiology of Aspergillus species causing keratitis in Mexico. Mycoses 62:144–151. https://doi.org/10.1111/myc.12855.
9. Keay L, Stapleton F, Schein O. 2007. Epidemiology of contact lens-related inflammation and microbial keratitis: a 20-year perspective. Eye Contact Lens 33:346–353. https://doi.org/10.1097/ICL.0b013e318157c49d.
10. Gupta M, Chandra A, Prakash P, Banerjee T, Maurya OPS, Tilak R. 2015. Fungal keratitis in north India; spectrum and diagnosis by Calcofluor white stain. Indian J Med Microbiol 33:462–463. https://doi.org/10.4103/0255-0857.158609.
11. Castano G, Mada PK. 2019. Fungal keratitis. StatPearls Publishing, Treasure Island, FL.
12. GAFFI. 2017. Priority fungal infections: hidden crisis. Gaffi, Geneva, Switzerland. https://gaffi.org/why/fungi-fungal-infections.
13. di Zazzo A, Antonini M, Fernandes M, Varacalli G, Sgrulletta R, Coassin M. 2020. A global perspective of pediatric non-viral keratitis: literature review. Int Ophthalmol 40:2771–2788. https://doi.org/10.1007/s10792-020-01451-z.
14. Khairallah SH, Byrne KA, Tabbara KF. 1992. Fungal keratitis in Saudi Arabia. Doc Ophthalmol 79:269–276. https://doi.org/10.1007/BF00158257.
15. Beltrán Rodríguez N, San Juan-Galán JL, Fernández Andreu CM, María Yera D, Barrios Pita M, Perurena Lancha MR, Velar Martínez RE, Illnait Zaragozí MT, Martínez Machín GF. 2019. Chronic pulmonary aspergillosis in patients with underlying respiratory disorders in Cuba—a pilot study. J Fungi 5:18. https://doi.org/10.3390/jof5010018.
16. Iqbal N, Irfan M, Mushtaq A, Jabeen K. 2020. Underlying conditions and clinical spectrum of chronic pulmonary aspergillosis (CPA): an experience from a tertiary care hospital in Karachi, Pakistan. J Fungi 6:41. https://doi.org/10.3390/jof6020041.
17. Krishnan S, Manavathu EK, Chandrasekar PH. 2009. Aspergillus flavus: an emerging non-fumigatus Aspergillus species of significance. Mycoses 52:206–222. https://doi.org/10.1111/j.1439-0507.2008.01642.x.
18. Frisvad JC, Hubka V, Ezekiel CN, Hong S-B, Nováková A, Chen AJ, Arzanlou M, Larsen TO, Sklenář F, Mahakarnchanakul W. 2018. Taxonomy of Aspergillus section Flavi and their production of aflatoxins, ochratoxins and other mycotoxins. Stud Mycol 91:37–59. https://doi.org/10.1016/j.simyco.2018.06.001.
19. Gonçalves SS, Stchigel AM, Cano JF, Godoy-Martinez PC, Colombo AL, Guarro J. 2012. Aspergillus novoparasiticus: a new clinical species of the section Flavi. Med Mycol 50:152–160. https://doi.org/10.3109/13693786.2011.593564.
20. Arastehfar A, Carvalho A, Houbraken J, Lombardi L, Garcia-Rubio R, Jenks JD, Rivero-Menendez O, Aljohani R, Jacobsen ID, Berman J, Osherov N, Hedayati MT, Ilkit M, Armstrong-James D, Gabaldón T, Meletiadis J, Kostrzewa M, Pan W, Lass-Flörl C, Perlin DS, Hoenigl M. 2021. Aspergillus fumigatus and aspergillosis: from basics to clinics. Stud Mycol 100:100115. https://doi.org/10.1016/j.simyco.2021.100115.
21. Donner M, Lichtemberg PSF, Doster M, Picot A, Cotty PJ, Puckett RD, Michailides TJ. 2015. Community structure of Aspergillus flavus and A. parasiticus in major almond-producing areas of California, United States. Plant Dis 99:1161–1169. https://doi.org/10.1094/PDIS-05-14-0450-RE.

22. Okun DO, Khamis FM, Muluvi GM, Ngeranwa JJ, Ombura FO, Yongo MO, Kenya EU. 2015. Distribution of indigenous strains of atoxigenic and toxigenic Aspergillus flavus and Aspergillus parasiticus in maize and peanuts agro-ecological zones of Kenya. Agric Food Secur 4:14. https://doi.org/10.1186/s40066-015-0033-5.
23. Garcia D, Ramos AJ, Sanchis V, Marín S. 2011. Modelling the effect of temperature and water activity in the growth boundaries of Aspergillus ochraceus and Aspergillus parasiticus. Food Microbiol 28:406–417. https://doi.org/10.1016/j.fm.2010.10.004.
24. Pasqualotto AC. 2009. Differences in pathogenicity and clinical syndromes due to Aspergillus fumigatus and Aspergillus flavus. Med Mycol 47:S261–S270. https://doi.org/10.1080/13693780802247702.
25. Bhabhra R, Askew DS. 2005. Thermotolerance and virulence of Aspergillus fumigatus: role of the fungal nucleolus. Med Mycol 43:87–93. https://doi.org/10.1080/13693780400029486.
26. Mead ME, Knowles SL, Raja HA, Beattie SR, Kowalski CH, Steenwyk JL, Silva LP, Chiaratto J, Ries LNA, Goldman GH, Cramer RA, Oberlies NH, Mitchell AP, Rokas A. 2019. Characterizing the pathogenic, genomic, and chemical traits of Aspergillus fischeri, a close relative of the major human fungal pathogen Aspergillus fumigatus. mSphere 4:e00018-19. https://doi.org/10.1128/mSphere.00018-19.
27. Medina A, Schmidt-Heydt M, Rodríguez A, Parra R, Geisen R, Magan N. 2015. Impacts of environmental stress on growth, secondary metabolite biosynthetic gene clusters and metabolite production of xerotolerant/xerophilic fungi. Curr Genet 61:325–334. https://doi.org/10.1007/s00294-014-0455-9.
28. Raffa N, Keller NP. 2019. A call to arms: mustering secondary metabolites for success and survival of an opportunistic pathogen. PLoS Pathog 15:e1007606. https://doi.org/10.1371/journal.ppat.1007606.
29. Lohmar JM, Puel O, Cary JW, Calvo AM. 2019. The Aspergillus flavus rtfA gene regulates plant and animal pathogenesis and secondary metabolism. Appl Environ Microbiol 85. https://doi.org/10.1128/AEM.02446-18.
30. Spikes S, Xu R, Nguyen CK, Chamilos G, Kontoyiannis DP, Jacobson RH, Ejzykowicz DE, Chiang LY, Filler SG, May GS. 2008. Gliotoxin production in Aspergillus fumigatus contributes to host-specific differences in virulence. J Infect Dis 197:479–486. https://doi.org/10.1086/525044.
31. Kjærbølling I, Vesth T, Frisvad JC, Nybo JL, Theobald S, Kildgaard S, Petersen TI, Kuo A, Sato A, Lyhne EK, Kogle ME, Wiebenga A, Kun RS, Lubbers RJM, Mäkelä MR, Barry K, Chovatia M, Clum A, Daum C, Haridas S, He G, LaButti K, Lipzen A, Mondo S, Pangilinan J, Riley R, Salamov A, Simmons BA, Magnuson JK, Henrissat B, Mortensen UH, Larsen TO, de Vries RP, Grigoriev I. v, Machida M, Baker SE, Andersen MR. 2020. A comparative genomics study of 23 Aspergillus species from section Flavi. Nat Commun 11:1106. https://doi.org/10.1038/s41467-019-14051-y.
32. Hedayati MT, Pasqualotto AC, Warn PA, Bowyer P, Denning DW. 2007. Aspergillus flavus: human pathogen, allergen and mycotoxin producer. Microbiology 153:1677–1692. https://doi.org/10.1099/mic.0.2007/007641-0.
33. Amaike S, Keller NP. 2011. Aspergillus flavus. Annu Rev Phytopathol 49:107–133. https://doi.org/10.1146/annurev-phyto-072910-095221.
34. Leal SM, Vareechon C, Cowden S, Cobb BA, Latgé JP, Momany M, Pearlman E. 2012. Fungal antioxidant pathways promote survival against neutrophils during infection. J Clin Invest 122:2482–2498. https://doi.org/10.1172/JCI63239.
35. Abad A, Victoria Fernández-Molina J, Bikandi J, Ramírez A, Margareto J, Sendino J, Luis Hernando F, Pontón J, Garaizar J, Rementeria A. 2010. What makes Aspergillus fumigatus a successful pathogen? Genes and molecules involved in invasive aspergillosis. Rev Iberoam Micol 27:155–182. https://doi.org/10.1016/j.riam.2010.10.003.
36. Fedorova ND, Khaldi N, Joardar VS, Maiti R, Amedeo P, Anderson MJ, Crabtree J, Silva JC, Badger JH, Albarraq A, Angiuoli S, Bussey H, Bowyer P, Cotty PJ, Dyer PS, Egan A, Galens K, Fraser-Liggett CM, Haas BJ, Inman JM, Kent R, Lemieux S, Malavazi I, Orvis J, Roemer T, Ronning CM, Sundaram JP, Sutton G, Turner G, Venter JC, White OR, Whitty BR, Youngman P, Wolfe KH, Goldman GH, Wortman JR, Jiang B, Denning DW, Nierman WC. 2008. Genomic islands in the pathogenic filamentous fungus Aspergillus fumigatus. PLoS Genet 4:e10000046. https://doi.org/10.1371/journal.pgen.1000046.
37. Kjærbølling I, Vesth TC, Frisvad JC, Nybo JL, Theobald S, Kuo A, Bowyer P, Matsuda Y, Mondo S, Lyhne EK, Kogle ME, Clum A, Lipzen A, Salamov A, Ngan CY, Daum C, Chiniquy J, Barry K, LaButti K, Haridas S, Simmons BA, Magnuson JK, Mortensen UH, Larsen TO, Grigoriev I. v, Baker SE, Andersen MR. 2018. Linking secondary metabolites to gene clusters through genome sequencing of six diverse Aspergillus species. Proc Natl Acad Sci U S A 115. https://doi.org/10.1073/pnas.1715954115.
38. Rudramurthy SM, Paul RA, Chakrabarti A, Mouton JW, Meis JF. 2019. Invasive aspergillosis by Aspergillus flavus: epidemiology, diagnosis, antifungal resistance, and management. J Fungi 5:55. https://doi.org/10.3390/jof5030055.
39. Houbraken J, Visagie CM, Frisvad JC. 2021. Recommendations to prevent taxonomic misidentification of genome-sequenced fungal strains. Microbiol Resour Announc 10:e01074-20. https://doi.org/10.1128/MRA.01074-20.
40. Fountain JC, Clevenger JP, Vaughn JN, Guo B. 2021. Lessons learned: the importance of biological curation. Microbiol Resour Announc 10:e00473-21. https://doi.org/10.1128/MRA.00473-21.
41. Fasoyin OE, Wang B, Qiu M, Han X, Chung K-R, Wang S. 2018. Carbon catabolite repression gene creA regulates morphology, aflatoxin biosynthesis and virulence in Aspergillus flavus. Fungal Genet Biol 115:41–51. https://doi.org/10.1016/j.fgb.2018.04.008.
42. Lan H, Wu L, Sun R, Yang K, Liu Y, Wu J, Geng L, Huang C, Wang S. 2018. Investigation of Aspergillus flavus in animal virulence. Toxicon 145:40–47. https://doi.org/10.1016/j.toxicon.2018.02.043.
43. Yang G, Cao X, Qin L, Yan L, Hong R, Yuan J, Wang S. 2020. Ssu72 regulates fungal development, aflatoxin biosynthesis and pathogenicity in Aspergillus flavus. Toxins (Basel) 12:717. https://doi.org/10.3390/toxins12110717.
44. Amaike S, Affeldt KJ, Yin W-B, Franke S, Choithani A, Keller NP. 2013. The bZIP protein MeaB mediates virulence attributes in Aspergillus flavus. PLoS One 8:e74030. https://doi.org/10.1371/journal.pone.0074030.
45. Liu Y, Zhang M, Xie R, Zhang F, Wang S, Pan X, Wang S, Zhuang Z. 2020. The methyltransferase AflSet1 is involved in fungal morphogenesis, AFB1 biosynthesis, and virulence of Aspergillus flavus. Front Microbiol 11:234. https://doi.org/10.3389/fmicb.2020.00234.
46. Lan H, Wu L, Fan K, Sun R, Yang G, Zhang F, Yang K, Lin X, Chen Y, Tian J, Wang S. 2019. Set3 is required for asexual development, aflatoxin biosynthesis, and fungal virulence in Aspergillus flavus. Front Microbiol 10:530. https://doi.org/10.3389/fmicb.2019.00530.
47. Chang P-K, Scharfenstein LL, Luo M, Mahoney N, Molyneux RJ, Yu J, Brown RL, Campbell BC. 2011. Loss of msnA, a putative stress regulatory gene, in Aspergillus parasiticus and Aspergillus flavus increased production of conidia, aflatoxins and kojic acid. Toxins (Basel) 3:82–104. https://doi.org/10.3390/toxins3010082.
48. Yang K, Qin Q, Liu Y, Zhang L, Liang L, Lan H, Chen C, You Y, Zhang F, Wang S. 2016. Adenylate cyclase AcyA regulates development, aflatoxin biosynthesis and fungal virulence in Aspergillus flavus. Front Cell Infect Microbiol 6:190. https://doi.org/10.3389/fcimb.2016.00190.
49. Fasoyin OE, Yang K, Qiu M, Wang B, Wang S, Wang S. 2019. Regulation of morphology, aflatoxin production, and virulence of Aspergillus flavus by the major nitrogen regulatory gene areA. Toxins (Basel) 11:718. https://doi.org/10.3390/toxins11120718.
50. Han X, Qiu M, Wang B, Yin W-B, Nie X, Qin Q, Ren S, Yang K, Zhang F, Zhuang Z, Wang S. 2016. Functional analysis of the nitrogen metabolite repression regulator gene nmrA in Aspergillus flavus. Front Microbiol 7:1794. https://doi.org/10.3389/fmicb.2016.01794.
51. Zhang F, Xu G, Geng L, Lu X, Yang K, Yuan J, Nie X, Zhuang Z, Wang S. 2016. The stress response regulator AflSkn7 influences morphological development, stress response, and pathogenicity in the fungus Aspergillus flavus. Toxins (Basel) 8:202. https://doi.org/10.3390/toxins8070202.
52. Yuan J, Chen Z, Guo Z, Li D, Zhang F, Shen J, Zhang Y, Wang S, Zhuang Z. 2018. PbsB regulates morphogenesis, aflatoxin B1 biosynthesis, and pathogenicity of Aspergillus flavus. Front Cell Infect Microbiol 8:162. https://doi.org/10.3389/fcimb.2018.00162.
53. Satterlee T, Entwistle S, Yin Y, Cary JW, Lebar M, Losada L, Calvo AM. 2019. rmtA-dependent transcriptome and its role in secondary metabolism, environmental stress, and virulence in Aspergillus flavus. G3 (Bethesda) 9:4087–4096. https://doi.org/10.1534/g3.119.400777.
54. Zhu Z, Ma G, Yang M, Tan C, Yang G, Wang S, Li N, Ge F, Wang S. 2021. Ras subfamily GTPases regulate development, aflatoxin biosynthesis and pathogenicity in the fungus Aspergillus flavus. Environ Microbiol 23:5334–5348. https://doi.org/10.1111/1462-2920.15626.
55. Yang G, Hu Y, Fasoyin OE, Yue Y, Chen L, Qiu Y, Wang X, Zhuang Z, Wang S. 2018. The Aspergillus flavus phosphatase CDC14 regulates development, aflatoxin biosynthesis and pathogenicity. Front Cell Infect Microbiol 8:141. https://doi.org/10.3389/fcimb.2018.00141.
56. Lan H, Sun R, Fan K, Yang K, Zhang F, Nie XY, Wang X, Zhuang Z, Wang S. 2016. The Aspergillus flavus histone acetyltransferase AflGcnE regulates morphogenesis, aflatoxin biosynthesis, and pathogenicity. Front Microbiol 7:1324. https://doi.org/10.3389/fmicb.2016.01324.
57. Chen X, Wu L, Lan H, Sun R, Wen M, Ruan D, Zhang M, Wang S. 2022. Histone acetyltransferases MystA and MystB contribute to morphogenesis and aflatoxin biosynthesis by regulating acetylation in fungus

Aspergillus flavus. Environ Microbiol 24:1340–1361. https://doi.org/10.1111/1462-2920.15856.
58. Cary JW, Harris-Coward PY, Ehrlich KC, Mack BM, Kale SP, Christy L, Calvo AM. 2012. NsdC and NsdD affect Aspergillus flavus morphogenesis and aflatoxin production. Eukaryot Cell 11:1104–1111. https://doi.org/10.1128/EC.00069-12.
59. Rui X, Kunlong Y, Elisabeth T, Zhiqiang G, Bei Z, Yinghang L, Zhenhong Z, Jun Y, Shihua W. 2022. Regulator of G protein signaling contributes to the development and aflatoxin biosynthesis in Aspergillus flavus through the regulation of Gα activity. Appl Environ Microbiol 88:e00244-22. https://doi.org/10.1128/AEM.00244-22.
60. Reverberi M, Punelli M, Scala V, Scarpari M, Uva P, Mentzen WI, Dolezal AL, Woloshuk C, Pinzari F, Fabbri AA, Fanelli C, Payne GA. 2013. Genotypic and phenotypic versatility of Aspergillus flavus during maize exploitation. PLoS One 8:e68735. https://doi.org/10.1371/journal.pone.0068735.
61. Amaike S, Keller NP. 2009. Distinct roles for VeA and LaeA in development and pathogenesis of Aspergillus flavus. Eukaryot Cell 8:1051–1060. https://doi.org/10.1128/EC.00088-09.
62. Tan C, Deng J-L, Zhang F, Zhu Z, Yan L-J, Zhang M-J, Yuan J, Wang S-H. 2021. CWI pathway participated in vegetative growth and pathogenicity through a downstream effector AflRlm1 in Aspergillus flavus. iScience 24:103159. https://doi.org/10.1016/j.isci.2021.103159.
63. Zhao Q, Pei H, Zhou X, Zhao K, Yu M, Han G, Fan J, Tao F. 2022. Systematic characterization of bZIP transcription factors required for development and aflatoxin generation by high-throughput gene knockout in Aspergillus flavus. J Fungi 8:356. https://doi.org/10.3390/jof8040356.
64. Brown SH, Scott JB, Bhaheetharan J, Sharpee WC, Milde L, Wilson RA, Keller NP. 2009. Oxygenase coordination is required for morphological transition and the host–fungus interaction of Aspergillus flavus. Mol Plant Microbe Interact 22:882–894. https://doi.org/10.1094/MPMI-22-7-0882.
65. Yang K, Shadkchan Y, Tannous J, Landero Figueroa JA, Wiemann P, Osherov N, Wang S, Keller NP. 2018. Contribution of ATPase copper transporters in animal but not plant virulence of the crossover pathogen Aspergillus flavus. Virulence 9:1273–1286. https://doi.org/10.1080/21505594.2018.1496774.
66. Chang P-K, Zhang Q, Scharfenstein L, Mack B, Yoshimi A, Miyazawa K, Abe K. 2018. Aspergillus flavus GPI-anchored protein-encoding ecm33 has a role in growth, development, aflatoxin biosynthesis, and maize infection. Appl Microbiol Biotechnol 102:5209–5220. https://doi.org/10.1007/s00253-018-9012-7.
67. Zhu Z, Yang M, Bai Y, Ge F, Wang S. 2020. Antioxidant-related catalase CTA1 regulates development, aflatoxin biosynthesis, and virulence in pathogenic fungus Aspergillus flavus. Environ Microbiol 22:2792–2810. https://doi.org/10.1111/1462-2920.15011.
68. Yao G, Zhang F, Nie X, Wang X, Yuan J, Zhuang Z, Wang S. 2017. Essential APSES transcription factors for mycotoxin synthesis, fungal development, and pathogenicity in Aspergillus flavus. Front Microbiol 8:2277. https://doi.org/10.3389/fmicb.2017.02277.
69. Yuan J, Li D, Qin L, Shen J, Guo X, Tumukunde E, Li M, Wang S. 2019. HexA is required for growth, aflatoxin biosynthesis and virulence in Aspergillus flavus. BMC Mol Biol 20:4. https://doi.org/10.1186/s12867-019-0121-3.
70. Nie X, Yu S, Qiu M, Wang X, Wang Y, Bai Y, Zhang F, Wang S. 2016. Aspergillus flavus SUMO contributes to fungal virulence and toxin attributes. J Agric Food Chem 64:6772–6782. https://doi.org/10.1021/acs.jafc.6b02199.
71. Zhang F, Geng L, Huang L, Deng J, Fasoyin OE, Yao G, Wang S. 2018. Contribution of peroxisomal protein importer AflPex5 to development and pathogenesis in the fungus Aspergillus flavus. Curr Genet 64:1335–1348. https://doi.org/10.1007/s00294-018-0851-7.
72. Wang P, Xu J, Chang P-K, Liu Z, Kong Q. 2022. New insights of transcriptional regulator AflR in Aspergillus flavus physiology. Microbiol Spectr 10:e00791-21. https://doi.org/10.1128/spectrum.00791-21.
73. Yuan X-Y, Li J-Y, Zhi Q-Q, Chi S-D, Qu S, Luo Y-F, He Z-M. 2022. SfgA renders Aspergillus flavus more stable to the external environment. J Fungi 8:638. https://doi.org/10.3390/jof8060638.
74. White EC, Hill JH. 1943. Studies on antibacterial products formed by molds. I. Aspergillic acid, a product of a strain of Aspergillus flavus. J Bacteriol 45:433–443. https://doi.org/10.1128/jb.45.5.433-443.1943.
75. Cox RH, Cole RJ. 1977. Carbon-13 nuclear magnetic resonance studies of fungal metabolites, aflatoxins, and sterigmatocystins. J Org Chem 42:112–114. https://doi.org/10.1021/jo00421a022.
76. Gould RO, Simpson TJ, Walkinshaw MD. 1981. Isolation AMD X-ray crystal structures of astellolides A and B, sesquiterpenoid metabolites of Aspergillus variecolor. Tetrahedron Lett 22:1047–1050. https://doi.org/10.1016/S0040-4039(01)82862-8.
77. Ren R, Chen C, Hu S, Ge H, Zhu W, Tan R, Jiao R. 2015. Drimane sesquiterpenoids from the Aspergillus oryzae QXPC-4. Chem Biodivers 12:371–379. https://doi.org/10.1002/cbdv.201400119.
78. Shinohara Y, Kawatani M, Futamura Y, Osada H, Koyama Y. 2016. An overproduction of astellolides induced by genetic disruption of chromatin-remodeling factors in Aspergillus oryzae. J Antibiot (Tokyo) 69:4–8. https://doi.org/10.1038/ja.2015.73.
79. Zhang C, Jin L, Mondie B, Mitchell SS, Castelhano AL, Cai W, Bergenhem N. 2003. Leporin B: a novel hexokinase II gene inducing agent from an unidentified fungus. Bioorg Med Chem Lett 13:1433–1435. https://doi.org/10.1016/s0960-894x(03)00153-7.
80. Cary JW, Uka V, Han Z, Buyst D, Harris-Coward PY, Ehrlich KC, Wei Q, Bhatnagar D, Dowd PF, Martens SL, Calvo AM, Martins JC, Vanhaecke L, Coenye T, De Saeger S, Di Mavungu JD. 2015. An Aspergillus flavus secondary metabolic gene cluster containing a hybrid PKS–NRPS is necessary for synthesis of the 2-pyridones, leporins. Fungal Genet Biol 81:88–97. https://doi.org/10.1016/j.fgb.2015.05.010.
81. Capon RJ, Skene C, Stewart M, Ford J, Richard AJ, Williams L, Lacey E, Gill JH, Heiland K, Friedel T. 2003. Aspergillicins A–E: five novel depsipeptides from the marine-derived fungus Aspergillus carneus. Org Biomol Chem 1:1856–1862. https://doi.org/10.1039/b302306k.
82. Pedras MSC, Morales VM, Taylor JL. 1993. Phomaligols and phomaligadiones: new metabolites from the blackleg fungus. Tetrahedron 49:8317–8322. https://doi.org/10.1016/S0040-4020(01)81915-3.
83. Büchi G, Francisco MA, Murray WV, Kachholz T, L Demain A, Blount JF. 1983. Aspersitin-a new metabolite of aspergillus parasiticus. Tetrahedron Lett 24:2527–2530. https://doi.org/10.1016/S0040-4039(00)81972-3.
84. Heathcote JG, Dutton MF. 1969. New metabolites of Aspergillus flavus. Tetrahedron 25:1497–1500. https://doi.org/10.1016/S0040-4020(01)82721-6.
85. Tsuda M, Mugishima T, Komatsu K, Sone T, Tanaka M, Mikami Y, Shiro M, Hirai M, Ohizumi Y, Kobayashi J. 2003. Speradine A, a new pentacyclic oxindole alkaloid from a marine-derived fungus Aspergillus tamarii. Tetrahedron 59:3227–3230. https://doi.org/10.1016/S0040-4020(03)00413-7.
86. Liu L, Bao L, Wang L, Ma K, Han J, Yang Y, Liu R, Ren J, Yin W, Wang W, Liu H. 2018. Asperorydines A–M: prenylated tryptophan-derived alkaloids with neurotrophic effects from Aspergillus oryzae. J Org Chem 83:812–822. https://doi.org/10.1021/acs.joc.7b02802.
87. Chen L, Zhang Q-Q, Hu X, Xia Q-W, Zhao Y-Y, Zheng Q-H, Liu Q-Y. 2014. Speradines BE, four novel tetracyclic oxindole alkaloids from the marine-derived fungus Aspergillus oryzae. Heterocycles 89:1662–1669. https://doi.org/10.3987/COM-14-13004.
88. Hu X, Xia Q-W, Zhao Y-Y, Zheng Q-H, Liu Q-Y, Chen L, Zhang Q-Q. 2014. Speradines F–H, three new oxindole alkaloids from the marine-derived fungus Aspergillus oryzae. Chem Pharm Bull (Tokyo) 62:942–946. https://doi.org/10.1248/cpb.c14-00312.
89. Uka V, Moore GG, Arroyo-Manzanares N, Nebija D, de Saeger S, Diana Di Mavungu J. 2017. Unravelling the diversity of the cyclopiazonic acid family of mycotoxins in Aspergillus flavus by UHPLC triple-TOF HRMS. Toxins (Basel) 9:35. https://doi.org/10.3390/toxins9010035.
90. Munday-Finch SC, Wilkins AL, Miles CO. 1996. Isolation of paspaline B, an indole-diterpenoid from Penicilium paxilli. Phytochemistry 41:327–332. https://doi.org/10.1016/0031-9422(95)00515-3.
91. TePaske MR, Gloer JB, Wicklow DT, Dowd PF. 1992. Aflavarin and β-Aflatrem: new anti-insectan metabolites from the sclerotia of Aspergillus flavus. J Nat Prod 55:1080–1086. https://doi.org/10.1021/np50086a008.
92. Masaki M, Chigira Y, Ohta M. 1966. Total syntheses of racemic aspergillic acid and neoaspergillic acid. J Org Chem 31:4143–4146. https://doi.org/10.1021/jo01350a062.
93. Okada Y, Taguchi H, Yokoi T. 1996. Amino acids and peptides. XLVII. Facile synthesis of flavacol, deoxymuta-aspergillic acid and optically active deoxyaspergillic acid from dipeptidyl aldehydes. Chem Pharm Bull 44:2259–2262. https://doi.org/10.1248/cpb.44.2259.
94. Ottria R, Casati S, Ciuffreda P. 2012. 1H, 13C and 15N NMR assignments for N-and O-acylethanolamines, important family of naturally occurring bioactive lipid mediators. Magn Reson Chem 50:823–828. https://doi.org/10.1002/mrc.3891.
95. Wishart DS, Knox C, Guo AC, Eisner R, Young N, Gautam B, Hau DD, Psychogios N, Dong E, Bouatra S, Mandal R, Sinelnikov I, Xia J, Jia L, Cruz JA, Lim E, Sobsey CA, Shrivastava S, Huang P, Liu P, Fang L, Peng J, Fradette R, Cheng D, Tzur D, Clements M, Lewis A, De Souza A, Zuniga A, Dawe M, Xiong Y, Clive D, Greiner R, Nazyrova A, Shaykhutdinov R, Li L, Vogel HJ, Forsythe I. 2009. HMDB: a knowledgebase for the human metabolome. Nucleic Acids Res 37:D603–D610. https://doi.org/10.1093/nar/gkn810.

96. Calvo AM, Hinze LL, Gardner HW, Keller NP. 1999. Sporogenic effect of polyunsaturated fatty acids on development of Aspergillus spp. Appl Environ Microbiol 65:3668–3673. https://doi.org/10.1128/AEM.65.8.3668-3673.1999.
97. Kawagishi H, Miyazawa T, Kume H, Arimoto Y, Inakuma T. 2002. Aldehyde dehydrogenase inhibitors from the mushroom Clitocybe c lavipes. J Nat Prod 65:1712–1714. https://doi.org/10.1021/np020200j.
98. Li Y-Y, Wang M-Z, Huang Y-J, Shen Y-M. 2010. Secondary metabolites from Phomopsis sp. A123. Mycology 1:254–261. https://doi.org/10.1080/21501203.2010.529583.
99. Zhang J, Lin X-P, Li L-C, Zhong B-L, Liao X-J, Liu Y-H, Xu S-H. 2015. Gliomasolides A–E, unusual macrolides from a sponge-derived fungus Gliomastix sp. ZSDS1-F7-2. RSC Adv 5:54645–54648. https://doi.org/10.1039/C5RA08559D.
100. Binder U, Maurer E, Lass-Flörl C. 2016. Galleria mellonella: an invertebrate model to study pathogenicity in correctly defined fungal species. Fungal Biol 120:288–295. https://doi.org/10.1016/j.funbio.2015.06.002.
101. Georgianna DR, Fedorova ND, Burroughs JL, Dolezal AL, Bok JW, Horowitz-Brown S, Woloshuk CP, Yu J, Keller NP, Payne GA. 2010. Beyond aflatoxin: four distinct expression patterns and functional roles associated with Aspergillus flavus secondary metabolism gene clusters. Mol Plant Pathol 11:213–226. https://doi.org/10.1111/j.1364-3703.2009.00594.x.
102. Drott MT, Rush TA, Satterlee TR, Giannone RJ, Abraham PE, Greco C, Venkatesh N, Skerker JM, Glass NL, Labbé JL, Milgroom MG, Keller NP. 2021. Microevolution in the pansecondary metabolome of Aspergillus flavus and its potential macroevolutionary implications for filamentous fungi. Proc Natl Acad Sci U S A 118. https://doi.org/10.1073/pnas.2021683118.
103. Mead ME, Steenwyk JL, Silva LP, de Castro PA, Saeed N, Hillmann F, Goldman GH, Rokas A. 2021. An evolutionary genomic approach reveals both conserved and species-specific genetic elements related to human disease in closely related Aspergillus fungi. Genetics 218:iyab066. https://doi.org/10.1093/genetics/iyab066.
104. Nargesi S, Jafarzadeh J, Najafzadeh MJ, Nouripour-Sisakht S, Haghani I, Abastabar M, Ilkit M, Hedayati MT. 2022. Molecular identification and antifungal susceptibility of clinically relevant and cryptic species of Aspergillus sections Flavi and Nigri. J Med Microbiol 71:1480. https://doi.org/10.1099/jmm.0.001480.
105. Reichert-Lima F, Lyra L, Pontes L, Moretti ML, Pham CD, Lockhart SR, Schreiber AZ. 2018. Surveillance for azoles resistance in Aspergillus spp. highlights a high number of amphotericin B-resistant isolates. Mycoses 61:360–365. https://doi.org/10.1111/myc.12759.
106. Negri CE, Gonçalves SS, Xafranski H, Bergamasco MD, Aquino VR, Castro PTO, Colombo AL. 2014. Cryptic and rare Aspergillus species in Brazil: prevalence in clinical samples and in vitro susceptibility to triazoles. J Clin Microbiol 52:3633–3640. https://doi.org/10.1128/JCM.01582-14.
107. Hara S, Fennell DI, Hesseltine CW. 1974. Aflatoxin-producing strains of Aspergillus flavus detected by fluorescence of agar medium under ultraviolet light. Appl Microbiol 27:1118–1123. https://doi.org/10.1128/am.27.6.1118-1123.1974.
108. Fatima S, Hu X, Gong R-H, Huang C, Chen M, Wong HLX, Bian Z, Kwan HY. 2019. Palmitic acid is an intracellular signaling molecule involved in disease development. Cell Mol Life Sci 76:2547–2557. https://doi.org/10.1007/s00018-019-03092-7.
109. Sexton AC, Howlett BJ. 2006. Parallels in fungal pathogenesis on plant and animal hosts. Eukaryot Cell 5:1941–1949. https://doi.org/10.1128/EC.00277-06.
110. St Leger RJ, Screen SE, Shams-Pirzadeh B. 2000. Lack of host specialization in Aspergillus flavus. Appl Environ Microbiol 66:320–324. https://doi.org/10.1128/AEM.66.1.320-324.2000.
111. Selvam RM, Nithya R, Devi PN, Shree RSB, Nila MV, Demonte NL, Thangavel C, Maheshwari JJ, Lalitha P, Prajna NV, Dharmalingam K. 2015. Exoproteome of Aspergillus flavus corneal isolates and saprophytes: identification of proteoforms of an oversecreted alkaline protease. J Proteomics 115:23–35. https://doi.org/10.1016/j.jprot.2014.11.017.
112. Evison SEF, Jensen AB. 2018. The biology and prevalence of fungal diseases in managed and wild bees. Curr Opin Insect Sci 26:105–113. https://doi.org/10.1016/j.cois.2018.02.010.
113. Ford S, Friedman L. 1967. Experimental study of the pathogenicity of aspergilli for mice. J Bacteriol 94:928–933. https://doi.org/10.1128/jb.94.4.928-933.1967.
114. Bastos RW, Valero C, Silva LP, Schoen T, Drott M, Brauer V, Silva-Rocha R, Lind A, Steenwyk JL, Rokas A, Rodrigues F, Resendiz-Sharpe A, Lagrou K, Marcet-Houben M, Gabaldón T, McDonnell E, Reid I, Tsang A, Oakley BR, Loures FV, Almeida F, Huttenlocher A, Keller NP, Ries LNA, Goldman GH. 2020. Functional characterization of clinical isolates of the opportunistic fungal pathogen Aspergillus nidulans. mSphere 5. https://doi.org/10.1128/mSphere.00153-20.
115. Bolger AM, Lohse M, Usadel B. 2014. Trimmomatic: a flexible trimmer for Illumina sequence data. Bioinformatics 30:2114–2120. https://doi.org/10.1093/bioinformatics/btu170.
116. Bankevich A, Nurk S, Antipov D, Gurevich AA, Dvorkin M, Kulikov AS, Lesin VM, Nikolenko SI, Pham S, Prjibelski AD, Pyshkin A. v, Sirotkin A. v, Vyahhi N, Tesler G, Alekseyev MA, Pevzner PA. 2012. SPAdes: a new genome assembly algorithm and its applications to single-cell sequencing. J Comput Biol 19:455–477. https://doi.org/10.1089/cmb.2012.0021.
117. Shumate A, Salzberg SL. 2021. Liftoff: accurate mapping of gene annotations. Bioinformatics 37:1639–1643. https://doi.org/10.1093/bioinformatics/btaa1016.
118. Hatmaker EA, Zhou X, Mead ME, Moon H, Yu J-H, Rokas A. 2020. Revised transcriptome-based gene annotation for Aspergillus flavus strain NRRL 3357. Microbiol Resour Announc 9. https://doi.org/10.1128/MRA.01155-20.
119. Jain C, Rodriguez-R LM, Phillippy AM, Konstantinidis KT, Aluru S. 2018. High throughput ANI analysis of 90K prokaryotic genomes reveals clear species boundaries. Nat Commun 9:5114. https://doi.org/10.1038/s41467-018-07641-9.
120. Simão FA, Waterhouse RM, Ioannidis P, Kriventseva E. v, Zdobnov EM. 2015. BUSCO: assessing genome assembly and annotation completeness with single-copy orthologs. Bioinformatics 31:3210–3212. https://doi.org/10.1093/bioinformatics/btv351.
121. Emms DM, Kelly S. 2019. OrthoFinder: phylogenetic orthology inference for comparative genomics. Genome Biol 20:238. https://doi.org/10.1186/s13059-019-1832-y.
122. Edgar RC. 2004. MUSCLE: multiple sequence alignment with high accuracy and high throughput. Nucleic Acids Res 32:1792–1797. https://doi.org/10.1093/nar/gkh340.
123. Capella-Gutiérrez S, Silla-Martínez JM, Gabaldón T. 2009. trimAl: a tool for automated alignment trimming in large-scale phylogenetic analyses. Bioinformatics 25:1972–1973. https://doi.org/10.1093/bioinformatics/btp348.
124. Nguyen L-T, Schmidt HA, von Haeseler A, Minh BQ. 2015. IQ-TREE: a fast and effective stochastic algorithm for estimating maximum-likelihood phylogenies. Mol Biol Evol 32:268–274. https://doi.org/10.1093/molbev/msu300.
125. Letunic I, Bork P. 2021. Interactive Tree Of Life (iTOL) v5: an online tool for phylogenetic tree display and annotation. Nucleic Acids Res 49:W293–W296. https://doi.org/10.1093/nar/gkab301.
126. Xu L, Dong Z, Fang L, Luo Y, Wei Z, Guo H, Zhang G, Gu YQ, Coleman-Derr D, Xia Q, Wang Y. 2019. OrthoVenn2: a web server for whole-genome comparison and annotation of orthologous clusters across multiple species. Nucleic Acids Res 47:W52–W58. https://doi.org/10.1093/nar/gkz333.
127. Bateman A, Martin MJ, O'Donovan C, Magrane M, Alpi E, Antunes R, Bely B, Bingley M, Bonilla C, Britto R, Bursteinas B, Bye-AJee H, Cowley A, da Silva A, de Giorgi M, Dogan T, Fazzini F, Castro LG, Figueira L, Garmiri P, Georghiou G, Gonzalez D, Hatton-Ellis E, Li W, Liu W, Lopez R, Luo J, Lussi Y, MacDougall A, Nightingale A, Palka B, Pichler K, Poggioli D, Pundir S, Pureza L, Qi G, Rosanoff S, Saidi R, Sawford T, Shypitsyna A, Speretta E, Turner E, Tyagi N, Volynkin V, Wardell T, Warner K, Watkins X, Zaru R, Zellner H, Xenarios I, et al. 2017. UniProt: the universal protein knowledgebase. Nucleic Acids Res 45:D158–D169. https://doi.org/10.1093/nar/gkw1099.
128. Blin K, Shaw S, Kloosterman AM, Charlop-Powers Z, van Wezel GP, Medema MH, Weber T. 2021. antiSMASH 6.0: improving cluster detection and comparison capabilities. Nucleic Acids Res 49:W29–W35. https://doi.org/10.1093/nar/gkab335.
129. Navarro-Muñoz JC, Selem-Mojica N, Mullowney MW, Kautsar SA, Tryon JH, Parkinson EI, De Los Santos ELC, Yeong M, Cruz-Morales P, Abubucker S, Roeters A, Lokhorst W, Fernandez-Guerra A, Cappelini LTD, Goering AW, Thomson RJ, Metcalf WW, Kelleher NL, Barona-Gomez F, Medema MH. 2020. A computational framework to explore large-scale biosynthetic diversity. Nat Chem Biol 16:60–68. https://doi.org/10.1038/s41589-019-0400-9.
130. Gilchrist CLM, Chooi Y-H. 2021. Clinker & clustermap.js: automatic generation of gene cluster comparison figures. Bioinformatics 37:2473–2475. https://doi.org/10.1093/bioinformatics/btab007.
131. Knowles SL, Roberts CD, Augustinović M, Flores-Bocanegra L, Raja HA, Heath-Borrero KN, Burdette JE, Falkinham JO, III, Pearce CJ, Oberlies NH. 2021. Opportunities and limitations for assigning relative configurations of antibacterial bislactones using GIAO NMR shift calculations. J Nat Prod 84:1254–1260. https://doi.org/10.1021/acs.jnatprod.0c01309.
132. Flores-Bocanegra L, Raja HA, Bacon JW, Maldonado AC, Burdette JE, Pearce CJ, Oberlies NH. 2021. Cytotoxic naphthoquinone analogues, including

heterodimers, and their structure elucidation using LR-HSQMBC NMR experiments. J Nat Prod 84:771–778. https://doi.org/10.1021/acs.jnatprod.0c00856.
133. El-Elimat T, Figueroa M, Ehrmann BM, Cech NB, Pearce CJ, Oberlies NH. 2013. High-resolution MS, MS/MS, and UV database of fungal secondary metabolites as a dereplication protocol for bioactive natural products. J Nat Prod 76:1709–1716. https://doi.org/10.1021/np4004307.
134. Paguigan ND, El-Elimat T, Kao D, Raja HA, Pearce CJ, Oberlies NH. 2017. Enhanced dereplication of fungal cultures via use of mass defect filtering. J Antibiot (Tokyo) 70:553–561. https://doi.org/10.1038/ja.2016.145.
135. Ries LNA, Beattie SR, Espeso EA, Cramer RA, Goldman GH. 2016. Diverse regulation of the CreA carbon catabolite repressor in Aspergillus nidulans. Genetics 203:335–352. https://doi.org/10.1534/genetics.116.187872.
136. Valero C, Goldman GH, Colombo AL, Rossato L, Bastos RW, Lagrou K. 2019. Potential of gallium as an antifungal agent. Front Cell Infect Microbiol 9:414. https://doi.org/10.3389/fcimb.2019.00414.
137. Cánovas D, Studt L, Marcos AT, Strauss J. 2017. High-throughput format for the phenotyping of fungi on solid substrates. Sci Rep 7:4289. https://doi.org/10.1038/s41598-017-03598-9.